The Development of a Printable Device with Gravity-Driven Flow for Live Imaging Glioma Stem Cell Motility

Yamilet Macias-Orihuela

Thesis submitted to the Faculty of the Virginia Polytechnic Institute and State University in partial fulfillment of the requirements for the degree of

Master of Science
In
Biomedical Engineering

Jennifer M. Munson, Committee Chair
Christopher B. Arena, Member
John L. Robertson, Member

December 5, 2022
Roanoke, VA

Keywords: Live microscopy, cell imaging, stereolithography, 3D printing, motility, heterogeneity, glioblastoma

The Development of a Printable Device with Gravity-Driven Flow for Live Imaging Glioma Stem Cell Motility

Yamilet Macias-Orihuela

ABSTRACT

The post-prognosis lifespan for those suffering with Glioblastoma (GBM) is approximately 13 months with current standard of care. Intratumoral heterogeneity is a common characteristic that hinders GBM treatment in the form of therapy resistant cell subsets and influence on cellular phenotypes. One cell subset in particular, glioma stem cells (GSCs), is frequently left behind in the brain parenchyma once the bulk of the tumor has been resected. Previous research has found that patient-derived GSCs displayed varying invasion responses with and without the presence of interstitial flow. Interestingly, GSCs from a single patient are heterogeneous, displaying differences among sub-colonies derived from the same parental line. To study the motility of cells under flow, PDMS microfluidics are commonly used. Unfortunately, this setup often involves active flow generation using pumps, limiting the number of cell lines that can be imaged at a time. To increase the throughput of GSC sub-colonies imaged simultaneously, we developed a bio-compatible, printable device fabricated to allow for passive, gravity-driven flow through a hydrogel that recapitulates the brain microenvironment, eliminating the need for pumps. Stereo lithography 3D printing was chosen as the manufacturing method for the device, and this facilitated design feature modification when prototyping, increased the potential complexity of future iterations, and avoided some of the hurdles associated with fabricating PDMS microfluidics. This printable imaging device allows for higher throughput live-imaging of cell lines to aid in the understanding of the relationships between intratumoral heterogeneity, invasion dynamics, and interstitial flow.

The Development of a Printable Device with Gravity-Driven Flow for Live Imaging Glioma Stem Cell Motility

Yamilet Macias-Orihuela

GENERAL AUDIENCE ABSTRACT

For those suffering with Glioblastoma, a high-grade brain cancer, the life span post treatment is approximately 13 months. The cells in this and many forms of cancer have physical and biological differences that make successfully eliminating the disease difficult. One of the cell types contributing to this are Glioma Stem Cells (GSCs) that are often left in brain tissue once most of the tumor has been surgically removed. Previous research has found that GSCs from different sources had different responses with and without the simulated or actual presence of flow in brain tissue. This was further complicated when different responses were observed in cells obtained when breaking apart one of the cell lines and propagating these into their own sub-colonies.

The current standard for studying the movement of cells under flow is by using compact chips made of a clear silicone rubber. The setup with microfluidics typically requires connection to external tubing and pumps to create flow and this limits the amount of cell types that can be imaged at a time. In order to monitor more cells at a time we created a 3D printable device that uses gravity for flow to go through a gel that mimics brain tissue and these cells of interest. Resin 3D printing was used to make these small devices so that they could be easily re-designed for other experimental purposes in the future. Hopefully this device could be used to more rapidly gain an understanding of cell movement in GBM and other disease models.

Para los que vinieron aquí con nada y me dieron todo. Los quiero tanto y gracias por inspirarme en mi educación y deseo a ayudar a los demás.
To my family, mentors, and friends for believing in me and making this journey possible.

Acknowledgements

Primeramente, quisiera darles las gracias a mis padres, Griselda y Jose, por darme todo su apoyo y cariño, especialmente durante estos pasados meses dedicados a acabar mi maestría. Siento que no hubiera llegado tan lejos sin ustedes y los amo mucho. Los aprecio tanto por inculcar en mi la habilidad de trabajar duro, no darme por vencida, y ser generosa con los demás. Para mis abuelos que tuve la dicha de conocer en esta vida y a los que siempre me cuidaron desde el cielo. Sé que en alguna manera yo recibí buena suerte de ustedes y espero que en algún lugar me estén mirando con orgullo. To my little brother and sister, Menyo and Yuli, for checking in on me while providing much needed comedic relief. Menyo, thanks for always giving me advice to stand up for myself and not let life walk all over me. Yuli, thank you for always lending me a sympathetic ear and being a bio nerd with me. Yessi, I feel like I should also include you in the sibling acknowledgments, thanks for being like another little sister to me and helping me stay sane when I felt the "eldest sister the family" role was becoming too much to handle. All those random late night video calls were very much needed energy boosts. I love you three so much and hope to continue helping each of you reach goals we never believed we could reach growing up. To the rest of my family that checked in on me and provided me with quality time whenever I was home from college I really appreciate each and every one of you. To Alberto, Monet, and Jenn for getting on zoom with the on my last day of writing this thesis. I really needed to see friendly faces on that day to get me through and I really appreciate you guys. Alberto thank you for being like a big brother to me and making sure I got all my Jenn thanks for always being there for me, checking on me when I was going through it, going to the movies with me when we needed a distraction and for being my "work wife" this last semester has really been intense and I am so happy we finally get to relax a bit. To all the cool, funny, sweet, smart, wonderful friends I made through

my undergraduate and graduate journey. I feel so overwhelmed trying to list all of you but I want you all to know I feel so grateful that I got to know each one of you and am so excited to spend time with you again soon. To my undergrad lab, Dr. Kylie Allen, Aleksei, Taylan and Kaleb, thanks for making my first research experience so amazing and inspiring me to want to stay in the lab even when things were not going my way. Though our time got cut short because of the pandemic I will always look back at the time in the lab fondly as I remember working together, funny moments, and all the new music I got to listen to while we worked on our experiments. Thank you so much Dr. Allen for showing me how exciting getting results in the lab can be and for being such a great mentor to me. I would like to give thanks to Claudia Brodkin for helping me get this experience. Claudia you have been one of the most influential women I got the luck of meeting as an undergraduate student. You have been so special to me as mentor, SHPE advisor, boss, friend, and almost like a second mother to me throughout this whole college experience. I appreciate you always looking out for me and its no wonder you have made such an impact on every single student that has crossed your path. I would also like to thank my SHPE familia for constantly exposing me to amazing people in engineering, I don't know if I would have made it through my undergraduate studies without having been a part of this amazing community. To my graduate lab, Dr. Jenny Munson, Aileen, Caleb, Cora, Conner, Gabriela, Jenn, Jessica, Joseph, Kinsley, Monet, Naciye, Peng, Rhea, Sam, Sarah, Savieay, Sharon, Yanping, and Zehra, thank you all for being so welcoming I will miss every one of you and am so excited to hear updates of all the cool work you all continue to do. Jenny thank you so much for giving me the opportunity to experience all of the amazing work that goes on in your lab, for constantly helping me remain excited on my projects, and over-all for being such an inspiration for me as a woman in STEM. Another special thanks to the lab "upperclassmen" Caleb, Cora, Kinsley, Monet, Naciye, and

Savieay for helping my cohort transition in during such a chaotic time, each of you was such an inspiration to me and I appreciate everything you taught me right from the start, whether it deals with scientific skills or how to get yourself through graduate school in one piece. Monet, I was so lucky to be paired up with you right from the start of my time in the lab and I will miss being your mentee so much. Though our work together led to many late-nights imaging and crowded time in the biosafety cabinet, I will now get to look back at those moments very fondly because you showed me the power of resilience each time. You have become such a great friend to me and I will miss our outings, but I know we will remain connected after I leave. I am so excited for you to start your lab and for more students to experience you as a role model and mentor. This project would not have been possible without the help of so many peers and collaborators. First I would like to thank my committee members Dr. Arena and Dr. Bob, thank you for all the input you provided me throughout my graduate studies and exciting ideas for future steps. Both of you made my interest for biomedical engineering flourish as an undergrad and I am so grateful for having had the opportunity to be your student. I would like to thank Hannah Musgrove from the Pompano lab for helping me identify the materials I would ultimately use to print my device and for her work studying these polymers which was such a crucial reference for me when I began working on making my device biocompatible. It was a great coincidence we got to attend the MPS conference in New Orleans together with Jenn this past summer and I will cherish the memories we made there. I can't wait to keep checking in on your research. Thank you so much Hannah Sheppard from the Vlaisavljevich Research Lab for taking the time to provide me with resources and train me on using the resin printer in Kelly. You were also so important in getting a good start on this project and wherever you go next is lucky to have you. I'd also like to thank you for being so kind and motivating at our last SBES symposium, it was really nice to have someone else to get

excited over device design with. Barkan Sidar, thank you so much for giving me ideas on passive flow generation at the MPS conference. It was great getting to meet you there and your brainstorming and intellect helped me get a lot closer to a successful final design of my device. Last, but not least, I would like to thank GEM and the New Horizons graduate scholars program for helping fund this experience and connecting me with so many students from diverse and similar background as me. Through these opportunites I was blessed to have gotten closer to two mentors, Renee Cloyd and Tremaine Waller. Thank you Trey for helping me with the GEM application process and motivating me through the graduate school application. I appreciate your mentorship throughout my whole time as a graduate student. Renee, I am so grateful I was able to build a connection with you through NHGS. You were also very significant part of my time at VT, I appreciate our frequent check-ins and all of the advice you gave me in trying to adjust to being a graduate student in the middle of a pandemic and as a first generation student. I will miss having a scheduled time to meet, but I plan on still swinging by your office and calling you to catch up.

Table of Contents

List of Figures

List of Tables

List of Abbreviations

- bFGF: Fibroblast growth factor-basic
- BSC: Biological safety cabinet
- CSC: Cancer stem cell
- ELDA: Extreme Limited Dilution Assay
- EGF: Epidermal Growth Factor
- EGFP: Enhanced green fluorescent protein
- EtHD1: Ethidium Homodimer I
- FRAP: Fluorescence recovery after photo-bleaching
- GBM: Glioblastoma Multiforme
- GSC: Glioma Stem Cells
- HA: Hyaluronic Acid, Hyaluronan
- HUVEC: Human Umbilical Vein Endothelial cell
- IFF: Interstitial fluid flow
- OA: Observation area, gel containing channel in IBIDI chip
- PBS: Phosphate buffered saline
- PDMS: Polydimethylsiloxane
- PEGDA: Poly(ethylene glycol) diacrylate
- PEGMEMA: Poly (ethylene glycol) methyl ethyl methacrylate
- PLA: Polylactic acid
- PVA: Polyvinyl alcohol
- LAP: Lithium phenyl-2,4,6-trimethylbenzoylphosphinate, photo-initiator for Photo-HA
- ROI: Region of interest
- STL: standard tessellation (or triangle) language, file format
- UV: Ultraviolet light
- μSL: Microstereolithography printing

Introduction

Broad Introduction to Cancer Invasion and Imaging Cell Motility

One of the hallmarks of cancer explored in hopes of elucidating the many forms of this disease is invasion and metastasis (Hanahan & Weinberg, 2000). This hallmark of cancer is one of the most well-known, yet how to study it in cancer cells efficiently and under physiological conditions in vitro remains a question. Once cancer cells have invasive and metastatic properties activated, they can spread cancer locally and distantly from the primary tumor mass, escaping any limitations in nutrients or space (Hanahan & Weinberg, 2011). The invasion-metastasis cascade begins with cells invading the local parenchyma and remaining in this adjacent tissue or colonizing distant tissues through the lymphatic or hematogenous systems. Regardless of the distance cells travel, this hallmark makes treating cancer arduous once the primary tumor is no longer the only point of concern.

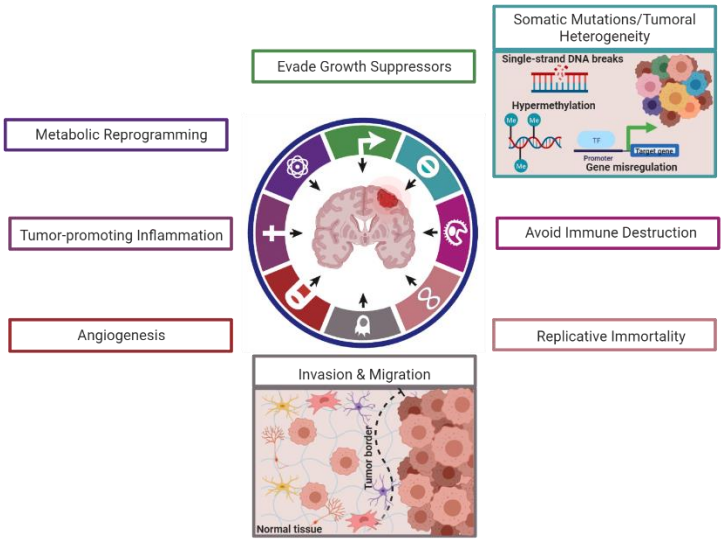

Figure 1. Hallmarks of cancer the Hallmarks of Cancer, circa 2011 (Hanahan & Weinberg, 2011). Courtesy of Monet Roberts, Ph.D. Created and modified with BioRender.com to highlight the hallmarks of interest.

One approach to further understanding invasion and metastasis is by targeting cancer cell motility (Wells et al., 2013). Though there are current limitations on how this is studied in vivo, some progress has been achieved in 2D and 3D in vitro models using live microscopy, also known as live cell imaging (Galarza et al., 2020). For the past couple of decades, the standard for live imagining required using microfluidic chips mostly made from Polydimethylsiloxane(PDMS) (McDonald & Whitesides, 2002; Narayanamurthy et al., 2020; Utada et al., 2005). PDMS is beneficial as it allows for optically transparent microfluidics, is permeable to oxygen and carbon dioxide, low cost, and easy to fabricate (Halldorsson et al., 2015; *Polydimethylsiloxane - an Overview | ScienceDirect Topics*, n.d.). Using microfluidic chips with cells also involves less difficulty when they are made of PDMS because the material is chemically inert and biocompatible with many cell types (Halldorsson et al., 2015). With live cell imaging, especially in 3D in vitro systems, PDMS can be adhered to glass or plastic slides because its material properties are compatible with plasma bonding (Xiong et al., 2014).

There are limitations to using PDMS; however, one of these is the difficulty in prototyping more complex designs. Without the ease of prototyping, adding flow to a system modeled by a PDMS microfluidic must be done by an external source or be delayed by the time it takes to produce a new design. For many biological applications, this material requires that labs have access to a clean room; this is especially true for more complex microfluidic structures where molds are needed for the PDMS to retain certain geometric features. Without a clean room, there is a risk of contaminants becoming encapsulated or leached by the material while curing (Aghamiri et al., 2021; de Almeida Monteiro Melo Ferraz et al., 2020).

A developing alternative to PDMS microfluidics is 3D printing (Bhattacharjee et al., 2016). 3D printing is already used to produce resin molds for PDMS and while this eliminates the need

for a clean room, this introduces the concern for leachates to be absorbed by the PDMS (de Almeida Monteiro Melo Ferraz et al., 2020). Leachates would pose a problem with using this fabrication alternative for biological functions, but with proper processing of printing materials, some biocompatibility can be achieved (Musgrove et al., 2022).

Development of 3D Printed Device for Live Imaging

Flow Generation

Most PDMS-based microfluidics with uniform height networks have achieved multiphase flow pattern formation in their channels by post-processing and localized surface functionalization. Flow patterns can also be achieved in microfluidics through multi-layered flow channel fabrication, but this requires meticulous alignment of all layers and experience (Männel et al., 2020). Since it is difficult to introduce the geometric features needed for controlled flow in PDMS microfluidics. flow is alternatively introduced to them by external actuators, fields, or power sources

Pressure-driven flow is the most common type of flow applied to microfluidics because it has the most well-characterized flow profile. Syringe pumps are often paired with microfluidics to generate this type of flow as they create reliable, stable flow and are easy to set up (Lake et al., 2017; Stone & Kim, 2001). However, with the addition of pumps, the compactness and portability of microfluidics are diminished, which are essential benefits of using microfluidics. In addition, these larger pumps often require connection to power sources while simultaneously being connected to microfluidics by tubing, limiting the configurations of a microfluidic on the microscope it will be imaged on as well as in the incubation system it must be in to keep the cells in viable conditions. These setups also involve issues such as gels not staying adhered to surfaces

with the pressure introduced by tubing attachment, tubing not being compatible with incubation systems for live imaging, and cavitation being introduced to the system.

To bypass the conflicts caused by pumps and other types of active flow created by external sources, focus can be placed on passively driven flow in microfluidics. Passive microfluidics attain flow by physical phenomena such as osmosis, capillary action, surface tension, pressure, gravity, hydrostatic flow, and vacuums. Microfluidics that achieve flow internally this way are easier to fabricate once a design has been established, require less expertise to operate, cost less, remain compact, and need no external power (Narayanamurthy et al., 2020). Various forms of passive flow, such as pressure, gravity, and hydrostatic pressure, were considered to design a microfluidic with pumpless flow. Pressure-driven flow relies on the force per unit area in fluids and can be equally divided in all directions. A force applied to one point of liquid will be transmitted to other points within the liquid. Gravity-driven flow is entirely driven by or assisted by gravity and can depend on the viscosity of the fluid or inlet height from the surface. Microfluidic flow driven by gravity would be expected to be continuous. Flow by hydrostatic pressure occurs because forces at equilibrium act on fluids with the same magnitude in all directions at any given point. Hydrostatic pressure increases in proportion to the depth of the fluid from the surface, meaning more downward force will be exerted from above when more fluid is added to the microfluidic. With all of these forms of passive flow, there are limits on the flow rate and on controlling continuous flow in the same way as pumps, but the advantages of using passive flow can outweigh these concerns. The main problem next comes with obtaining passive flow in a higher throughput manner so that more samples can be exposed to it without being hindered by the level of complexity that can be achieved when prototyping different structures with this material's current fabrication methods.

Manufacturing Method

Extrusion Printing

The first alternative method considered for fabricating a live imaging device was extrusion printing because it was the most accessible. The extrusion printer and materials were readily available in our facility. Extrusion is the most commonly known method of 3D printing. With this process, a polymer filament, such as polylactic acid (PLA), goes through plastic deformation as force or heat is applied. The pressure causes the material to flow through an orifice or die to adopt the cross-sectional profile of said outlet. The shape printed is retained with the proper materials, environment, and settings (Hill, 2005). The 3D printers used had the aforementioned die in a printer head that could simultaneously move and lay extruded filament in the desired geometry. The filament would be deposited on a heated glass plate for a smooth bottom surface and easy removal. Layers would be deposited in layers as the printer head moved up or the printer plate moved down. Properly orienting the design and adding support material would be needed for larger versions of this device. For just the single chamber prints, however, the device only had to be printed with the length of the wells perpendicular to the print plate so that these would not collapse while printing. For expanding the design, it was thought that this method would be ideal because polyvinyl alcohol (PVA), a water-soluble synthetic polymer, was available as a support material (*Poly Vinyl Alcohol - an Overview | ScienceDirect Topics*, n.d.). PVA would not impact the print since it could just be dissolved off, and using it while printing the actual device with another polymer would be possible with the two printer heads on the Ultimaker extrusion printers used.

Quality settings for extrusion printers included layer height, which on the Ultimaker ranged from 0.06 mm to 0.2 mm. The thicker layers allowed for quicker prints, but the finer layers would

ultimately lead to the resolution desired for the microfluidic this device would replace. Upon test printing, there were issues with the finest layer selection due to the filament stringing and concern that the surface roughness allowed for leaks and improper gel adhesion.

Stereolithography Printing

A complete switch to another printing method was done to address resolution concerns with extrusion printing. The lab had access to a microstereolithography (μSL) resin printer. μSL is a versatile tool that can be used to obtain small features with high resolution in a short process time (Männel et al., 2020). In μSL, a photo-curable resin is polymerized layer by layer with ultraviolet light (UV) with the capacity to produce complex microstructures. There is a rapidly increasing amount of publications that demonstrate an interest in the fabrication of microfluidic devices utilizing μSL due to the higher level of accessibility provided with this method (Bhattacharjee et al., 2016; Femmer et al., 2015; Gong et al., 2017; Jans et al., 2019; Männel et al., 2020).

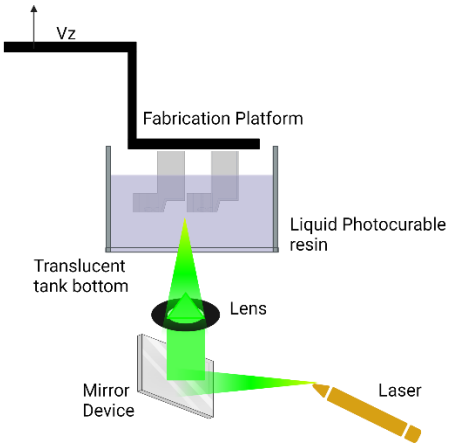

Figure 2. "Bat Configuration" in Stereolithography Resin Printing (Hwang et al., 2018). Modified using BioRender.com

This method of 3D printing functions “upside down” compared to an extrusion printer; this is commonly referred to as in “bat” configuration. The process begins with a resin-filled tank aligned below a build plate where the print will hang. The plate is immersed in the resin, while a UV laser beaming from beneath the translucent tank will activate the photo-crosslinking component in the resin into the desired geometry for each layer. The UV light is focused enough to obtain intricate design features on prints. Print orientation and the addition of supports are crucial to retaining desired features because the resin is not fully hardened with the laser curing and upon removal. Where this would not be as much of a concern with extrusion printing, printing with resin requires the use of supports to avoid cupping. Cupping is a phenomenon where uncured resin flows into openings, creating an area of pressure susceptible to damage and other impacts on unhardened outer portions of the print (*Cupping Blowout*, n.d.; *Preventing Suction Cups in PreForm*, n.d.; Fleck et al., 2021; Musgrove et al., 2022). Enough supports must also be added so that the print is securely hanging from the build plate; otherwise, new layers will not successfully attach with nothing to hold onto. Taking precautions to orient the print with the smallest design features, in this case the channels for flow, facing away from the build plate, also ensures that removing the supports does not impair the device's function. The exact resin chosen will also impact the final resolution of the device.

Material Selection

Detailed information on the ingredients in commercial resins is not available to address specific non-biocompatible components directly or manipulate other material properties (Männel

et al., 2020). With the lack of transparency of commercially available resins, lab-made resins became a potential alternative if a commercial resin was not found to use with cells.

Resins commonly used with stereolithography printing are typically not biocompatible, especially in comparison to PDMS microfluidics which have already been shown to be biocompatible, cytocompatible, and non-genotoxic. New formulations of resin need to reach similar levels of compatibility for μSL printed microfluidics to be applied in the same ways and to be as versatile as PDMS devices (Männel et al., 2020). Labs have developed libraries of homemade resins based on varying acrylate formulas. Poly (ethylene glycol) diacrylate (PEGDA) and poly (ethylene glycol) methyl ethyl methacrylate (PEGMEMA) containing resins were identified as compatible for making cell culture platforms. The aforementioned polymers allowed mammalian cells exposed to them to retain both their viability and proliferative capabilities (Männel et al., 2020; McAvoy et al., 2018). Post-print processing steps were introduced to achieve higher levels of viability. Processing included a washing step with phosphate buffered saline (PBS) before cell culture to ensure that unbound or unconsumed components of resin, including that of the base material, the ultraviolet (UV)-absorber, and the photo-initiator, did not leak out from the printed material during long-term cell exposure and impact the cells. With these methods, Human Umbilical Vein Endothelial cells (HUVECs) could grow in the presence of multiple resins in a similar shape and size compared to cells grown in the standard culturing environment (Männel et al., 2020). Since HUVECs could survive after exposure to processed resin, it is believed that more robust cancer cells would also be able to withstand this exposure.

Implementation of Device to Study GBM

This device was developed with an application in mind, which contributed to the features on the overall design specification list, to more efficiently study cancer cell motility under flow. Glioblastoma Multiforme (GBM) is a tumor that originates from supportive glial cells and is the most common and aggressive primary brain tumor in adults. GBM is so aggressive that it is assigned the highest grade from the World Health Organization classification of brain tumors. An estimated 10k + patients succumb to this grade IV tumor annually in America (*About Glioblastoma*, n.d.; *Gliomas | Johns Hopkins Medicine*, n.d.; Wirsching et al., 2016). Even after the current standard of care is applied, survival rates remain dismal, with the current five-year survival rate being 5.8% and the ten-year survival rate dropping to 0.71% (Tan et al., 2020; Tykocki & Eltayeb, 2018). Survival and mortality statistics have not changed significantly for decades because progress in treatment has not extended life expectancy past a few months (*About Glioblastoma*, n.d.). The poor prognosis of GBM can be attributed to a high rate of recurrence, intratumoral heterogeneity, the infiltrative-migratory behavior of glioblastoma cells to vital brain structures, and the difficulty in delivering drugs to the central nervous system (Jackson et al., 2019; Kim et al., 2015).

The rapid progression of this cancer can be attributed to resistance to therapy and unavoidable recurrence (Jackson et al., 2019). The current standard of care has been developed mainly for primary GBM; this involves surgical resection of the bulk of the tumor and a concurrent application of radiotherapy with the chemotherapeutic drug, Temozolomide. The addition of the latter two treatment components has doubled the two-year survival rate to 27%, but the overall prognosis remains with poor results (Duffau, 2017; Tykocki & Eltayeb, 2018). Currently, there is no well-defined treatment for recurrence. Drugs such as Lomustine have emerged as possible treatments for recurrence, but there is limited evidence of their success (Weller & le Rhun, 2020).

The rapid progression of this type of cancer and resistance to therapy work in combination with recurrence along with several factors such as uncontrollable cell growth rate; therefore, preventing it is the only course of action that can lead to success with patients (Jackson et al., 2019).

Treatment resistance due to heterogeneity has impacted the ability to target cancer cells on the molecular and cellular levels; this is especially true regarding the variance between cancer stem cells (CSCs) (Jackson et al., 2019; Kim et al., 2015). CSC modeling dates back to functional studies on leukemia (Bonnet & Dick, 1997; Furth & Kahn, 1937; Lapidot et al., 1994). The results from these studies began the search for CSCs in other cancer types, including brain cancer (Hemmati et al., 2003; Singh et al., 2003, 2004). The CSC hypothesis models a significant contributor to the poor prognosis of GBM. This hypothesis acknowledges that tumors are not homogenous masses of neoplastic cells but ecosystems of diverse cell populations. Often left in the infiltrative edge of a tumor after the bulk is resected, glioma stem cells can be considered a type of stem cell at the "apex" of heterogeneity (Gimple et al., 2019; Munthe et al., 2016). Glioma stem cells, like other CSCs, are both functionally defined by and distinguished from the tumors, Gliomas, they descend from. Understanding these types of cells and their ability to recapitulate tumor heterogeneity can help mitigate their ability to aid in the recurrence of Gliomas (Gimple et al., 2019).

The infiltrative-migratory behavior of cancer cells can be understood by honing in on the oncological role of flow in the brain, GBM, and how this contributes to the spread of a tumor. There are three ways for the spread of cancer to occur. Cancer cells can disseminate to other parts of the body through the hematogenous or lymphatic system. For cancer cells to reach either of these systems, they must first "dislodge from the primary tumor" and travel through the interstitium (Swartz & Lund, 2012). The interstitium or interstitial space is found outside of blood

and lymph vessels; consists of connective and supportive structures; does not include cells as part of this space, and consists of a fluid phase that is mostly plasma from capillaries. There is flow here, despite being outside vasculature, caused by diffusion or pressure. The flow in this space, especially next to the tumor environment, is present because of the larger amount of pressure found in a tumor than in normal, healthy tissue (Swartz & Lund, 2012). A disruption in the transport and drainage of interstitial fluid causes increased pressure in and near the tumor environment. The increased intratumoral pressure increases interstitial flow, which promotes flow away from the tumor (Wagner & Wiig, 2015). Cancer cells interacting with this type of flow experience effects that impact their invasive behavior, such as creating chemokine gradients that promote invasion and migration (Munson & Shieh, 2014).

The ultimate purpose of this device would be to image what happens to glioma stem cells when combining factors such as heterogeneity and the infiltrative-migratory behavior of cancer cells to gain clarity on GBM. The effects of interstitial fluid flow have been studied directly on glioma stem cells from multiple patients and of varying niches to find that multiple mechanisms might be involved in differential invasion responses to interstitial fluid flow (Kingsmore et al., 2016). The previous paper focused on interpatient heterogeneity for cell behavior, and further in vivo studies mapped the heterogeneity of interstitial fluid flow within and around individual glioblastomas (Kingsmore et al., 2018). After achieving these findings, one of the next steps in understanding the relationship of flow with Glioblastoma is to look at intrapatient cell behavior. Sub-colonies developed from individual patient cell lines might display differences in response to flow within their parental groups. Studying this with prior methods can be hindered by time, the desire to compare cell behavior in flow to that in static conditions, and the number of sub-colonies that could be derived from a singular patient-derived cell line. A high throughput device like the

one proposed is desired to facilitate this next step in understanding the impact of interstitial fluid flow on GBM.

Methods

Methods for device development

Single Chamber Design

Dimensions from a 384-well plate were used as the base of this design, with the plan to make an imaging device as high throughput as possible and the knowledge that at least three units would be necessary for a gel to be exposed to flow passively. The 3D model encapsulating the cells of interest would be contained by one unit in the form of a hydrogel. The remaining device units would be an inlet that holds the necessary volume of media to introduce a pressure head for flow and an outlet that collects the media that traveled through the hydrogel. Single chambers that included these three components and were connected by horizontally aligned channels on the bottom were designed on Inventor Professional (Autodesk).

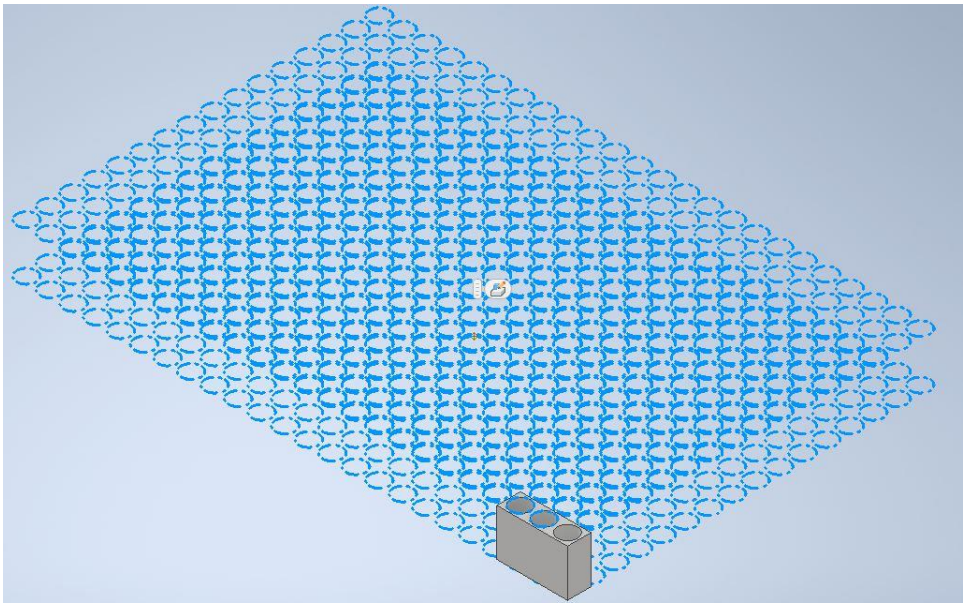

Figure 3. Single Chamber dimensions in relation to 384 well plate.

In order to have a device with the capacity to image a similar amount of conditions as can be studied on a 96-well plate static flow invasion assay, dimensions from a 384-well plate were used. The well diameters in the single chamber design were in the range of the diameter for the wells in 384 well plates and that of the plate inserts used to hold the gels in 96-well plate assays (*Corning® 3374 HTS Transwell® 96 Permeable Support Culture Plate System With*, n.d.; *Corning | Materials Science Technology and Innovation*, n.d.). The center-to-center spacing was the same as in the 384-well plate used for size reference (*Corning | Materials Science Technology and Innovation*, n.d.). The height of the device was kept similar to that of the well plates without a lid for initial viability and flow tests.

The channel connecting the wells and the overall structure of the middle well varied among the initial three designs. All three Single chamber design versions (V2, V3, and V4) were tested for flow and potential use issues. Looking at each of these designs from the top or sides, they might

all look like the same three well segments of a 386 well plate, but the inside and bottom view shown in **Figure 4** reveals the imaging design variations amongst them.

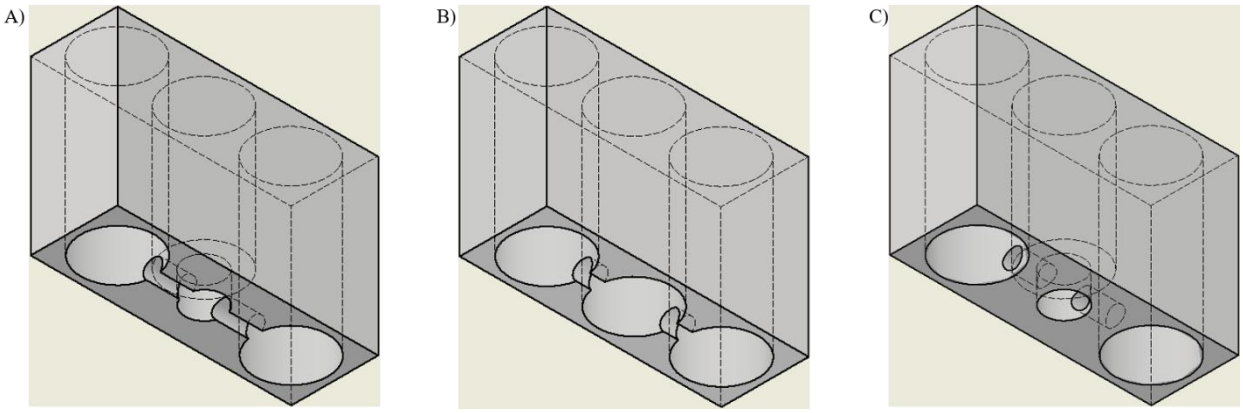

Figure 4. Initial single chamber designs.

In version 2 (V2) of the single chamber design, the middle well narrows down on the bottom, where the channels connect it to the inlet and outlet wells. The channels in V2 and V3 were not complete cylinders and were fully exposed to the dish or slide the chambers were attached to for imaging. This feature might have been helpful for visual flow tests as the whole trajectory of flow would be within visible range on the microscope. However, the issue with the exposed channel came with silicone application for attachment; it took a lot of work to control how the silicone spread when placing the chambers onto another surface. Despite measures to limit excess silicone, such as using a needle syringe, plugs, and an Axio Zoom microscope (Zeiss) for more precise application, the silicone would not consistently distribute evenly. When too much silicone got into the channels or even covered the bottom of the middle well, liquid would not flow between the wells, and leaks or flow blockages would often inhibit the function of these chambers. Functional issues were typically found less with V3 than V2, possibly due to the middle chamber being larger on the bottom and allowing the sealant to spread around those edges. V4 had the least

amount of flow issues when only liquid was introduced to the system, the channel connecting the wells was entirely enclosed by resin, so this might have inhibited sealant from leaking in.

Besides the integrity of the seal with the device, the application of silicone also impacted imaging. Less ROIs (regions of interest) could be imaged in V2 and V4 because of the smaller well diameter on the bottom. Reduced visibility was made worse with the addition of silicone for all designs. When plugs were introduced to cover the wells while imaging, there was a significant decrease in visibility for V2 and V4, this problem did not occur with V3 because some light could still get through to the bottom, allowing cells to remain visible.

Other adhesion methods and materials were attempted to bypass the issues with silicone, but ultimately this attachment method would prove to be the best and most accessible for the time being. Despite the issues faced at this point of the design process, it was determined that V3 would be the best single chamber to improve upon. V3 was the base for iterations that would lead to a multi-chamber design that had desired flow rates not just with liquid in the device but also with the addition of a gel in the middle chamber.

Flow Tests

Designs were tested for flow using the hydrogel recipe previously used to study the impact of interstitial fluid flow (IFF) on GSCs (Kingsmore et al., 2016). The recipe contained 0.12 % collagen, 0.2% HA, media, and a thiol-reactive PEGDA crosslinker. The collagen in the hydrogel was introduced as a 0.3% Collagen solution consisting of Collagen type 1 (Thermo Fisher Scientific), 1N NaOH, Sterile Milli Q H20, and 10x PBS was made over ice. GSC media and 1x PBS were used interchangeably as the fluid phase of the hydrogel. Fifty μL hydrogels were applied to each resin device iteration's middle or flow well. The hydrogels were incubated at 37°C for 30 minutes to begin crosslinking. After the initial set, the gels were rehydrated with 20 μL of media

and allowed to fully crosslink for another three hours at 37°C before the final amount of media was placed on the setup for static and flow conditions. Experiments for flow were run for 16 to 18 hours in the incubator. The end volume of media on the inlet and outlet was compared to the initial values to determine if flow occurred or if changes in media levels were due to other reasons.

Iterations

Modifications to the single chamber designs began after no flow was detected. These different versions included the increased height of the inlet well. No flow occurred; the increase later in height and total media on the inlet would eventually work but just having one tall well did not provide enough volume of media to create flow through the gel. The connecting channels were expanded to be longer but on the vertical axis. This modification ended up creating leaks in between the chambers. There was also concern that the gel's cross-sectional area would be too exposed to the pressure introduced by the media and that this would cause the gel to be pushed out of place. This idea was successfully revisited later by elongating the channel cross area on the horizontal axis, instead of vertically, for the final version of the device. The inclusion of an outlet well was also tested, believing that media was needed on the outlet to induce hydrostatic pressure and create flow. Media could have created more resistance for flow if it was held in a small well, so pieces were printed that ended right after the middle well. The designs with no outlet were placed and attached inside the wells of 12-well plates. A media layer was applied around the devices to determine if this could drive flow out of the device. This feature was modified and tried in the final multi-chambered design as the reservoir outlet. The composition of the hydrogel was also considered as a reason for no flow, where concerns were that the HA introduced enough hydrodynamic resistance to inhibit flow through the small channels. Parallel attempts with

different device versions were used with a decreased HA concentration or a complete replacement of HA with collagen to test if HA inhibited flow. In these scenarios, the changes in the hydrogel recipe did not make much of a difference.

Computer Aided Design

Inventor

All designs and modifications to the device were done using Inventor Professional (Autodesk). Inverted versions of designs for the resin device and the Ibidi microfluidic chip were also made on Inventor using device measurements or by combining the original design with a "blank" version to make a mold. The .stl files of inverted versions were uploaded to finite element analysis software as the geometry for fluid flow simulations. If Inventor designs were incompatible with the software above, Inventor was used to obtain measurements for recreating the negative space in the printed designs.

COMSOL Flow Simulation on Resin Device

For the Resin Device finite element flow simulation, the geometry was initially obtained from inverted versions of the device design created on Inventor. These files were run on finite element analysis, solver, and simulation software (COMSOL Multiphysics). The design's negative space was oriented so that the back of the device is the large inlet tank, the front of the device is the outlet wells, the left is where the small outlet tank is, and the right is the outlet wells. Unfortunately, this geometry had to be recreated directly on COMSOL from the Inventor file dimensions because the original file's channel-to-well interface was incompatible with the mesh generated.

A new origin was selected after recreating the geometry to facilitate boundary selection. The new origin was placed at the bottom left corner of the front of the inlet tank. The remaining structures were created here and moved to their respective positions based on measurements from the Inventor file. Once the geometry was fully established, this simulation was run to test for issues before boundary planes were applied to the design to help with material division later on and have the correct flow simulation in media or the gel matrix phase. A total of three planes were created "behind gel", in "front of gel", and on "top of gel" to later isolate the region we expected the hydrogel to be placed on.

Darcy's law, $q = -\frac{k}{\mu}\nabla p$, was used as the governing physics applied to the fluid flow simulation through the resin device. Free and porous media flow was set as the physics in this module. Custom material properties, shown in **Table 1**, were applied to the domain constrained to mimic the hydrogel. The remaining domains in the device had water applied as the material due to these properties being comparable to the media used for flow generation.

Other boundary conditions on this device involved the application of wall conditions to the surfaces where no flow would be assumed. A fine mesh was applied to the geometry of the device. Gravity was included in the flow simulation and when calculating the inlet pressure for different volumes of media. For the resin device, 8mL of media was added for the final run of experiments, so the volume of this in the inlet design was calculated along with the potential pressure this would create using the hydrostatic pressure equation, $p = \rho g h$. One increased value at the maximum volume of the device and several decreasing volumes of inlet media were also simulated in case the device could be shortened in future experiments. The calculated pressures were applied to the middle of the inlet channel, where the height used in calculating was determined. The pressure on

top of the inlet, the gel, and the outlet was assumed to be atmospheric. The superficial velocity at the center of the hydrogel at the same z-plane as that of the inlet pressure calculation was solved using the results module of the flow simulation.

Table 1. Material Properties and Constants for COMSOL

Parameter	Variable	Value	Unit	Source
Density of Hydrogel	ρ	1007	kg/m^3	Manufacturer of HA , assumed similar for Photo HA
Dynamic Viscosity of Hydrogel	μ	9.79E-04	Pa*S	Manufacturer of HA
Gravity	g	9.81	m/s^2	Constant
Inlet Pressure	p_0	238.9	Pa	Calculated pressure head on Inlet for 8mL of media
Outlet Pressure	p	0	Pa	Atmospheric Constant
Permeability of Hydrogel	κ	3.19E-14	m^2	(Munson et al., 2013)
Porosity of Hydrogel	ε	0.3	1	(Linninger et al., 2005)
Temperature	T	310.15	K	Physiological Temperature

COMSOL Flow Simulation on IBIDI Chip

Flow was also simulated on COMSOL for the inverse of one IBIDI chip chemotaxis chamber. The hydrogel in the geometry of this chip was isolated by creating two planes and placing them parallel to the length of the OA on the left and right sides. The space between these planes had the properties of the hydrogel material applied to it as a singular domain. The remaining domains were interpretations of the reservoirs beside the OA, and the properties of water were applied here to represent media. Circular openings on the reservoir wings represented the inlet and outlet ports. The same governing physics and boundary conditions as the resin device were applied to the chip. Volumetric flow rate, $Q=v \times A$, was used instead of pressure for flow simulation in

this module setup. The volumetric flow rate was calculated based on the potential flow velocities selected on the syringe pumps and the cross area of the ports. This velocity was only applied to the inlet ports. The outlet ports had the boundary condition of atmospheric pressure applied to them, as in this simulation, it was assumed there would be no withdrawal pumps. The flow rates tested were initially much larger than what was believed could be applied to the gel without dislodging it or pushing it out of the OA. The flow rate achieved by this in the center of the gel simulation was recorded, and iterations of the simulation with decreasing inlet flow rates were completed until this value reached desired velocities based on IFF models (Kingsmore et al., 2016; Munson et al., 2013; Swartz & Lund, 2012).

Device Preparation

3D Printing

Iterations of the device created on Inventor were converted to .stl files to be oriented on the 3D printing software (PreForm, Formlabs). Dimensions were scaled on the software to ensure that these matched what was created on Inventor. In order to get the best resolution and smoothest finish on prints, the smallest layer size available on PreForm was selected for each material used, 0.025 mm (Formlabs Clear V4) and 0.050 mm (Formlabs Biomed Clear V1). Flow devices and covers were oriented so that the sides with essential details, i.e., the well-connecting channels and the well plugs, were facing away from the build plate. Necessary features needed to be facing out so that the addition of supports would not compromise design functions. The devices were oriented

so that their longer sides were parallel to the mixer side of the Formlabs printer. In addition, each piece's 'bottom face' was oriented 15° from the build plate on the y-axis to ensure the well cavities were at an angle. Print designs were not positioned flat on the build plate to avoid cupping damage resulting from the resin not fully curing, creating a suction force (Formlabs). Once the designs were oriented as desired, supports were manually added in touchpoint sizes ranging from 0.40 mm to 0.75 mm with a full-sized raft on the base. Adjusting the support settings allowed for easier removal from the build plate and led to less excess material when removing supports.

Post Processing protocol for Biocompatibility

Resin prints were cleaned immediately after removing them from the base plate. Supports were carefully removed using tweezers with a slight twisting motion so that features of the device would not be broken off before the final cure. The fully uncured layer of resin on prints was rinsed off by submerging pieces in 99% Isopropyl alcohol (Millipore Sigma) and leaving this on a rocker at 100 rpm for 1 hour and 20 minutes as recommended by the manufacturer (Formlabs). The resin was allowed to dry for no more than a few hours to avoid cracking in the next step. A final cure was applied to the resin in FormCure (Formlabs) at 60°C for 20 minutes to strengthen and improve the finished surface of the device.

The device was attached to histology slides for imaging using clear silicone waterproof sealant (Loctite). After the silicone hardened, the seal was tested using purified H2O (Milli-Q); if the seal was good, more H2O was added to cover the whole device and leach any remaining uncured silicone particles for at least two hours. While the leaching occurred in sterile water, the whole device was sterilized using the UV light in the BSC for 30 minutes. After leaching, the water was removed and the device was sterilized again upside down. The final post-processing step was

a 24-hour, 50°C, 1x PBS bath to remove as many remaining resin particulates as possible before the device contacts cells. The bath temperature and solution were chosen based on the clear resin's stability from Formlabs and prior biocompatibility testing (Musgrove et al., 2022).

Methods for Implementation

Glioma Stem Cell Culture

Glioma stem cells were kindly gifted by Jaku Godlewski to Benjamin Purow. Multiple GSCs (G2, G34, and G62) were derived and cultured following a previously established protocol (Lee et al., 2006). The GSCs cultured for experiments were selected based on their invasive response, or lack thereof, to interstitial flow (Kingsmore et al., 2016). Culturing of GSCs consisted of growing them in non-treated suspension flasks in a media recipe of Neurobasal medium, N2 supplement, B27 supplement without Vitamin A, and GlutaMAX (Thermo Fisher Scientific). GSCs were cultured until confluent spheroids were formed after approximately one week of adding decreasing amounts of human recombinant endothelial (EGF) and fibroblast (bFGF) growth factors (Thermo Fisher Scientific) every other day. Cells were kept in a humidified incubator under the conditions: 21% Oxygen, 5% Carbon Dioxide, and 37 °C (Cornelison et al., 2022). Upon reaching confluency for experimental needs, cells were spun down at 1100 rpm for 5 minutes, and spheroids were broken apart by triturating 150 to 200 times using a 200 μL Micropipette (Eppendorf). GSC sub-colonies were isolated by Dr. Monet Roberts using an extreme limiting dilution assay and scaled up for use in these experiments.

3D Hydrogel Tumor Microenvironment model

Cells were encapsulated in an HA-collagen hydrogel meant to mimic the stiffness and composition of the brain tumor extracellular matrix (Delpech et al., 1993; Munson et al., 2013). This gel mixture's mechanical properties allowed for flow rates like what has been reported in vivo to be achieved (Munson et al., 2013). Two recipes of this HA-collagen matrix gel were used to develop the live-imaging device.

GSC Viability in Resin Device

It was necessary to test the device's biocompatibility early in its development. Viability tests were done on GSC lines that were (G34) and were not (G2) flow responsive (Kingsmore et al., 2016). Cells were encapsulated in the hydrogel model at 1 million cells per milliliter concentration and media was added for static conditions after crosslinking. HyStem® hydrogel kit (Advanced BioMatrix) was used as the base of the gel. The thiol-modified hyaluronan in this kit was prepared before experiments by resuspending it in degassed, deionized water and rocking it in a cold room overnight. A 0.3% Collagen solution consisting of Collagen type 1 (Thermo Fisher Scientific), 1N NaOH, Sterile Milli Q H20, and 10x PBS was made over ice to inhibit the collagen from cross-linking. The hydrogel recipe contained 0.12 % collagen, a media resuspension of GSCs, 0.2% hyaluronan, and a thiol-reactive PEGDA crosslinker. All components were thoroughly mixed, and 50 μL of hydrogel was applied to a well in the resin device. The hydrogels were incubated at 37°C for 30 minutes; after the initial set, the gels were rehydrated with 20 μL of media, allowed to fully crosslink for an additional three hours at 37°C, before the final amount of media was placed on the set up for static and flow conditions. The device holding the cell and hydrogel mixture was incubated for 18 hours. After incubating, excess media was removed. A viability assay was applied to the hydrogels using a LIVE/DEAD™ Cell Imaging Kit (Invitrogen,

Thermo Fisher Scientific). This dual probed assay contained a live cell indicator (Calcein, AM) which could permeant all cells, and a dead cell indicator (BOBO-3 Iodide) that would be activated when reaching the permeable nucleus of a dead cell. The two components of the assay would be mixed, and 50 μL of this mix was applied to each gel at room temperature for 30 minutes. Excess liquid was removed, and the gels were removed from the device to be set between a histology slide and cover slip for imaging.

The live/dead labeled cells were imaged on an inverted microscope (ZEISS Axio Observer) at 100x magnification. Cells were counted, and %viable= number of live cells/total number of cells × 100.

Resin Device Imaging Set Up

Preliminary images of unlabeled cells in brightfield were taken on resin devices attached to a petri dish or a histology slide. G2 and G34 Cells at a 1 million per milliliter density were encapsulated in 50 μL gels. It was determined that placing the device on a histology slide and placing the imaging configuration on the slide holder inside the microscope's incubation chamber would allow for more consistent imaging than having been set up in a petri-dish. Positions for imaging were selected and categorized on Zen microscopy software (Zeiss).

Resin Device Live-Imaging

Live imaging was done on GSC sub-colonies of interest on the final iteration of the device. The same density of cells and volume of gel were used as in the standard imaging setup. To better understand cell movement, the cells were stained using Vybrant™ DiD Cell-Labeling Solution (Thermo Fisher Scientific). This cell labeling technique had been used previously when imaging

sub-colonies in static conditions, and the resin would not autofluoresce in the same channel as the dye (Musgrove et al., 2022). Labeled cells were encapsulated in the photo-HA hydrogel. The hydrogel consisted of 0.12 % collagen, a media resuspension of GSCs, 0.4% photo-crosslinkable HA (PhotoHA®-Stiff, Advanced BioMatrix), and 0.008% LAP (Sigma-Aldrich). The PhotoHA and photo-initiator, LAP, percentages were based on manufacturer and collaborator recommendations and stiffness testing to match this up with the other hydrogel recipe used. The collagen was introduced in a 0.3% solution of Collagen type 1 (Thermo Fisher Scientific), 1N NaOH, Sterile Milli Q H20, and 10x PBS was made over ice. The same volume of gel as used in static flow invasions assays, 50 uL, was placed in the middle wells of the device. The gels were crosslinked under a 170 mA current of UV light (Thorlabs) that was placed about 145 mm from the base of the device for 45 seconds. The UV light crosslinked the HA, and the device was incubated for 30 minutes at 37°C for the collagen to crosslink.

All the gels had 20 μL of media applied on top because the gels in static conditions would not be exposed to more media for the duration of the experiment. The device's design only had channels connecting half of the hydrogels to media inlets and outlets. The media inlet reservoir contained 8 mL of GSC media. The outlets shaped like circular wells received 20 μL of media each, and the outlet shaped like a rectangle received 100 μL. A plug cover was made of the same resin as the device, and this was placed over the gel-containing wells and the outlets. Parafilm was used to cover the whole device while transporting it to the microscope and imaging.

The device was placed in a stage-top incubator for live cell imaging (Ibidi). The incubator chamber bottom and lid were connected to a controller to maintain optimal conditions (37°C, 5.2% CO2, 20% O2, and 80% relative humidity) for cell viability. Settings were allowed to equilibrate on the incubator chamber before placing the device on it and while selecting imaging ROIs. Images

in static conditions were previously taken for five ROIs per condition at 100x magnification. Only three ROIs were imaged in each gel inside the resin device to accommodate the smaller imaging area. An image was taken of the cells every 15 minutes for 16 hours for two passages of each sub-colony of interest.

The most centered ROI was selected to be analyzed for each condition because this had the most amount of clarity or the least amount of silicone. With the final design of this device, there were two technical replicates of each condition since there were two chambers for each of the four conditions. The conditions imaged are listed from the device's left to right side: Static open, flow open, static closed, and flow closed. The conditions labeled “open” were those on the side of the device with the rectangular reservoir as the outlet, and those labeled “closed” were on the side with wells as outlets.

Ibidi µ-Slide Chemotaxis Microfluidic Imaging Set Up

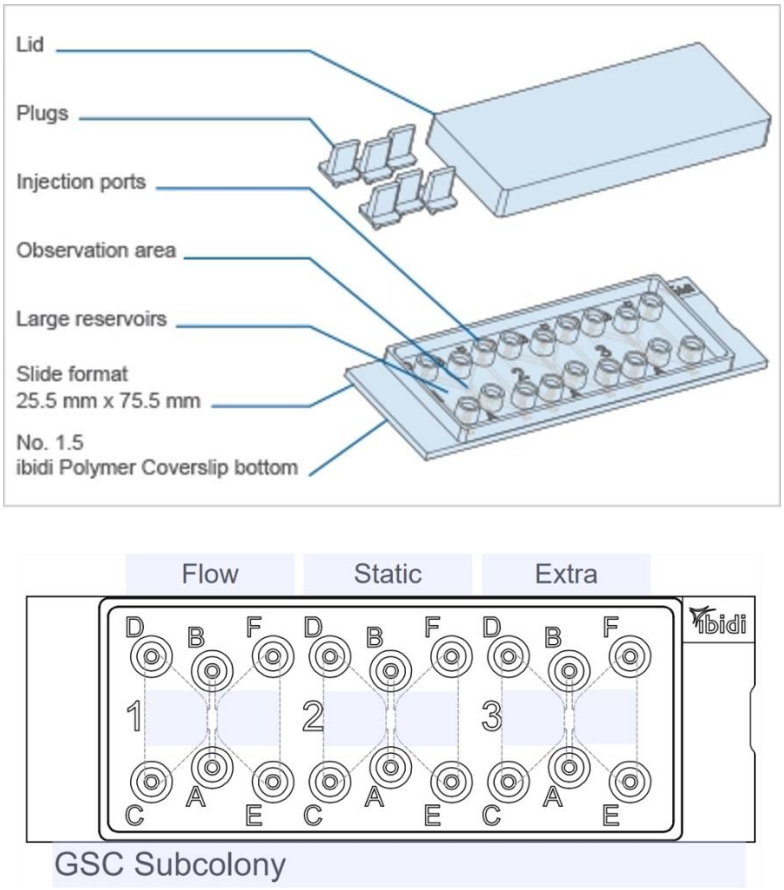

Figure 5. Microfluidic set up for imaging and feature labels (IBIDI).

An alternative setup consisting of a bio-compatible microfluidic chip was developed to image the sub-colonies of interest and to compare to the protocol developed with the resin device. This alternative setup consisted of a repurposed µ-Slide Chemotaxis assay chip (IBIDI) which would hold the GSC hydrogel. An infusion and a withdrawal syringe pump (Fusion 200, Chemyx), each loaded with two 5 mL Luer-lock syringes (BD), were used to introduce active flow. The two main components were connected and sealed using silicone tubing of a 0.8 mm inner diameter (IBIDI), female Luer lock connectors (IBIDI), and parafilm (Genesee).

Cells were passaged and counted as previously described. In this setup, Hoechst 33342 (20mM, Thermo Fisher Scientific) was used to label the nuclei of cells at a 1:2000 dilution in

media before these were added to the hydrogel mixture. The PhotoHA hydrogel mixture was used for the final optimization and imaging trials of the GSCs. It was determined that a cell density of 10 million cells per 1 mL of gel was ideal for this imaging setup. Before anything was added to the chip, plugs from the IBIDI kit were inserted into injection ports C, D, F, and E to create pressure that would inhibit the gel from leaking out of the observation area (OA). This gel was applied and distributed to the OA ports A and B, per the recommendations of IBIDI, using beveled tips provided with their chip. The HA in the gel was crosslinked in the BSC with UV light before placing plugs on the OA ports. The chip was then incubated for 30 minutes at 37°C for the collagen to crosslink before media was introduced to the system.

GSC media was applied to the reservoirs beside the OA individually, while the opposing reservoir ports contained plugs so that the addition of media would not shear through the gel. Plugs were replaced in all ports to perform preliminary imaging of the chip and select the two chemotaxis chambers with the best cell distribution for imaging under static and flow conditions. The ports on the chamber selected for flow had Luer-lock connectors attached to them with a sealing layer of parafilm. The Luer lock connectors had plugs inserted into them when adding more media to the system to remove any air bubbles. The syringes on the pump were filled with media containing 10mM of a HEPES buffer solution (Irvine Scientific); this concentration was chosen based on the standard concentrations of HEPES used in cell culture (*Cell Culture Media Supplements | Thermo Fisher Scientific - US*, n.d.). HEPES was added to the media in the syringes to aid pH regulation since, in previous runs, this media was not exposed to the CO2 in the stage top incubator for the same purpose. The syringes were then connected to Luer-locks and silicone tubing. Any air in the syringes or tubing was removed before finally connecting the tubes to the flow condition chamber on the IBIDI chip. Tubes leading to the pump that would push media through from the infusion

pump were attached to the chip first, then the plugs on the opposite reservoir were removed to connect the withdrawal pump tubing.

The IBIDI chip was set in the slide holder on the microscope's stage-top for imaging. Once everything was secured, the pumps were turned on to introduce media at a flow rate of 0.1 µL/min through the gel. The flow rate was selected based on previous microfluidic pump flow setups used in the lab and COMSOL simulations of flow in this device. The pumps ran for at least 30 minutes as ROIs were selected and conditions in the incubator returned to ideal ranges. The cells in the static and flow chamber OAs were imaged in five ROIs at 200x total magnification for 16 hours in 15-minute increments. At the end of the experiment, the device was checked to ensure that the infusion tubing did not come off overnight and that there were little air bubbles in either reservoir that could impair flow.

Cell Motility Image Processing and Analysis

For the images taken at 100x magnification, one ROI was analyzed; for the resin device, this was selected based on how clear the region was. All of the single visible cells in an ROI were counted. The live imaging obtained on the Axio Observer were .czi files converted to .tif files. The .tif versions of the image stacks were converted from 16-bit images to RGB color images to be compatible with Celleste Image Analysis Software (Thermo Fisher Scientific). In the final form of stacks, these could be viewed as videos with adjustable brightness and contrast levels on Celleste.

The migrating cells for each ROI were identified as those that moved >2 cell body lengths. The % migration, or invasion, = amount of migrating cells/ total amount of cells × 100. Tracks

were created on the Celleste software to determine the directionality and displacement of the migrating cells.

Results

Final Multi-chamber device design

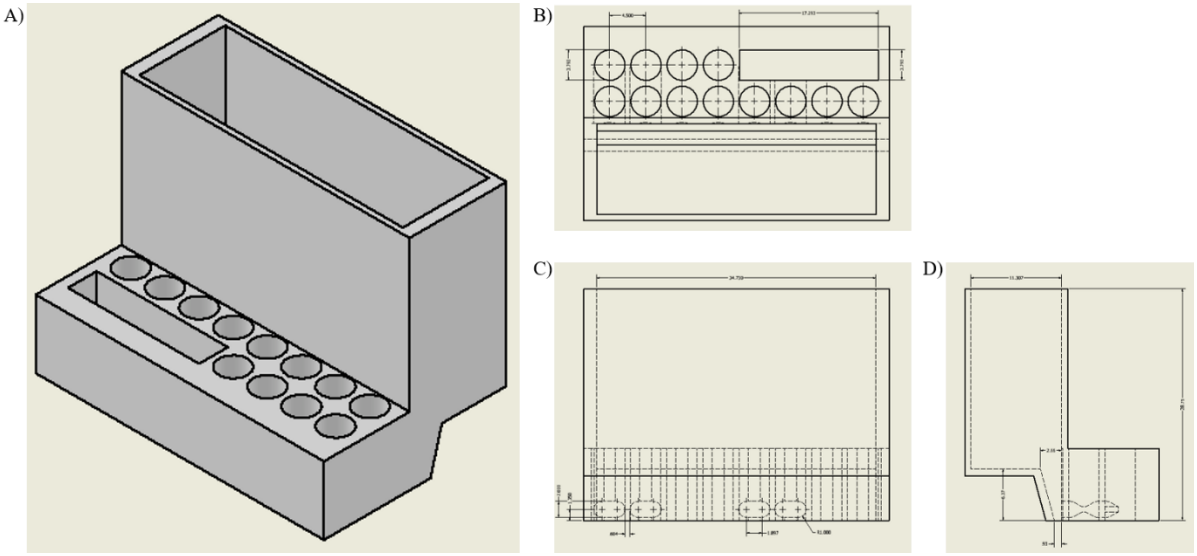

Figure 6. Inventor drawing of final multi-chamber device design. A) The full isometric projection of the final design showing the tops of the tank inlet (back), the middle chamber where the hydrogels will be set, the reservoir outlet (front left), and the four well outlets (front right). B) The top view shows the dimensions of each of the openings. All openings, except the inlet, are uniform through to the bottom of the device. C) The back slice of the device shows the dimensions of the horizontally oriented oval slot channels that connect the wells. Only the "flow" wells had channels added to them. D) The side profile of the device displays how the channels run through the middle wells from the inlet to the outlet for flow generation. This view also shows the narrowing of the inlet tank, a design feature that, along with the smaller channel cross-section, would increase pressure from the media in the tank and lead to flow.

After multiple iterations of the resin device design were produced and tested, the final version was designed to have a maximum height of 28.75 mm to fit in an incubation chamber and a slide holder fitted on the microscope used for live imaging. The wells containing the hydrogel model of the brain remained the same dimension as in the single chamber design as this size gave good results in imaging gels with similar dimensions as those in a 96-well plate (50 μL gel with 1 million cells/mL). All four components of the single chamber- the inlet, middle chamber, outlet,

and connecting channels- were modified in designs to determine if this would allow for flow not only with liquid but also through a gel.

Two different outlet designs were used to determine if these created different flow velocities through the gel. Half of the flow chambers were connected to wells as the outlets, and the other half was connected to a rectangular reservoir. The static chambers were not connected to anything and stood alone.

All the flow chambers were connected to the same inlet reservoir, which could hold a significantly higher volume of media. A higher amount of media would introduce more pressure into the system, which would be enough for the media to transport through the hydrogel matrix. The reservoir was designed to be uniform in width on top and taper off to a smaller volume towards the bottom where the channels were connected; this feature was meant to promote hydrostatic flow. The increased pressure from media volume and design features were meant to work with gravity to introduce flow into the chambers connected to this component by channels.

The channel geometry was changed for the final iteration of this device from a partial or full circular cross-section with a 0.5 mm diameter to a horizontally expanded oval slot. This modification was attempted before with a vertically elongated oval channel, but this design did not consider gel displacement and ultimately allowed for gaps on the top for liquid to move through instead of gel. The current device has horizontal slots with the same vertical width as the original chambers, 0.5 mm, and wider horizontal width of 2.897 mm. The channel was widened so that a larger cross-section would promote flow through a hydrogel. This channel was placed low on the device so that gel displacement would not create openings for fluid movement above the gel while still using a 50 μL volume of gel like in the original channel design. The channel was not placed on the bottom of the device to avoid issues seen with V2 and V3 of the single chamber design

when using silicone to attach to a glass slide. The measurement of the distance of the new channel opening to the bottom, 0.35 mm, was comparable to that of the V4 single chamber, 0.3 mm. Successful flow was seen with this chamber design through a hydrogel in conjunction with the modified inlet design.

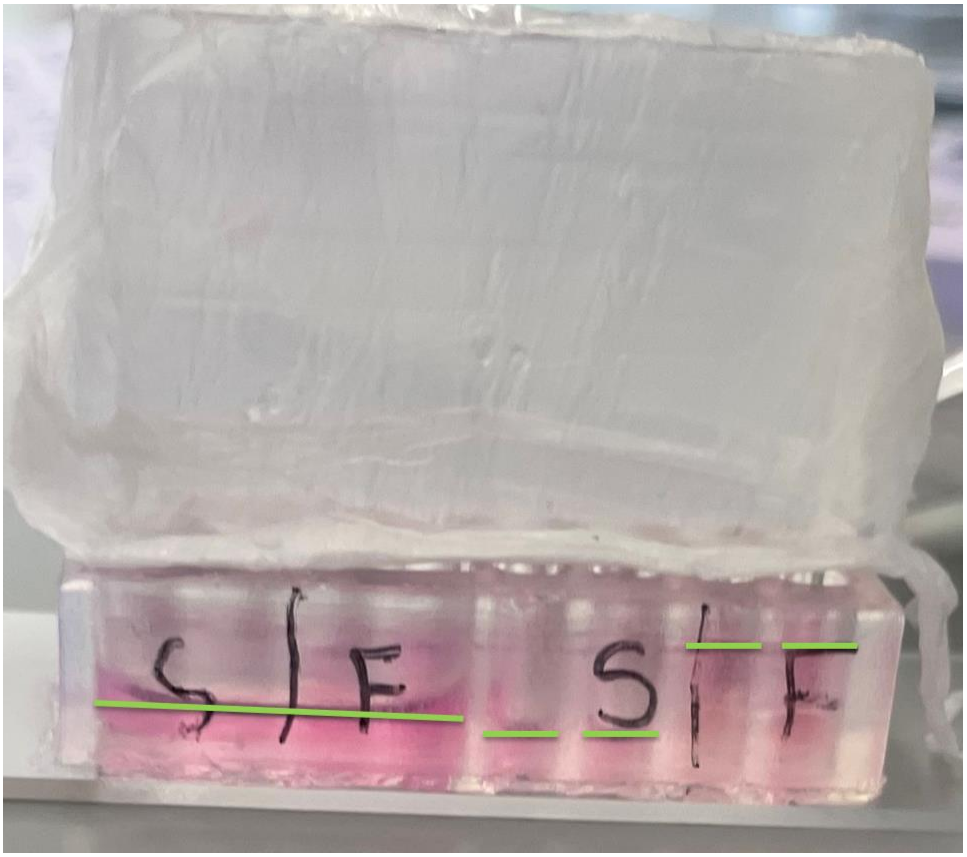

Figure 7. Media levels after overnight incubation of hydrogel.

Table 2. Media volume measurements at the start and end of "flow" during overnight incubation.

	Volume of Media (µL)				
	Reservoir Outlet	Well Outlet			
	All	Static		Flow	
Start	100	20	20	20	20
End	~225-250	17	18	52	40

COMSOL modeling of flow through the chamber

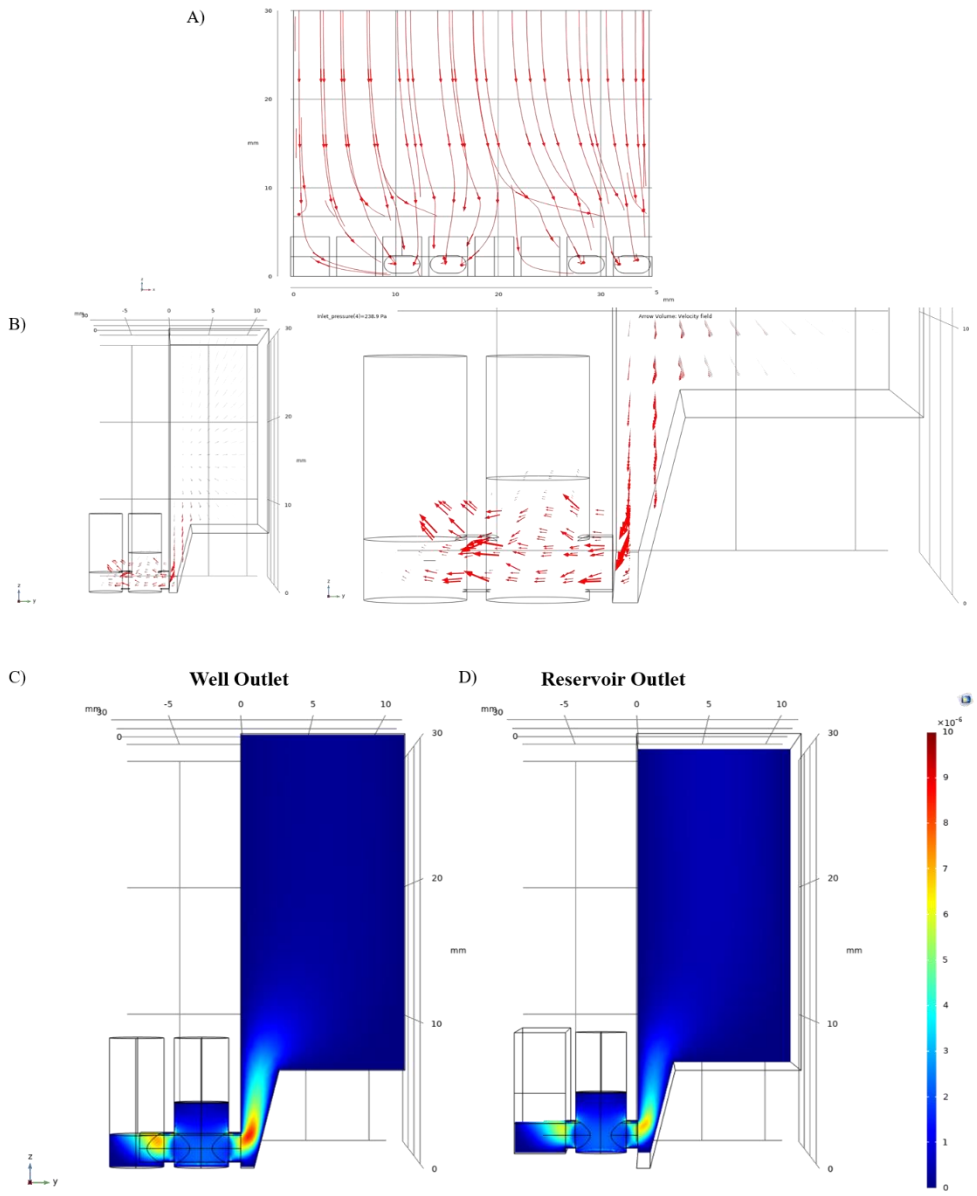

Figure 8. COMSOL passive fluid flow simulation of 8 mL of media from the inlet, through hydrogel in the middle, well, to each outlet design. A) Arrows streamlines show the trajectory of flow from the front view of the device. B) The side profile and zoomed in version of this better displays the proportioned arrow streamlines for velocity. This perspective shows the direction of flow across the hydrogel. C) A slice of the velocity magnitude gradient was taken right at the middle XY-coordinates of a flow well connected to a well outlet. This is the rightmost flow well shown on (A). D) Shows the same data as (C) for a flow well connected to the reservoir outlet. This is from the middle of the second flow well from the left on (A). The gradient legend on (C) and (D) is for the velocity magnitude in m/s.

The simulation of flow on COMSOL successfully ran to match the scenario of flow in the live-imaging device, as shown by **Figure 8(A)** where the flow trajectory begins at the top of the inlet down to the channel openings. The simulation was run at multiple pressures calculated based on the device's geometry and height from the center of the channel cross-section to the theoretical top of the media. **Figure 8** only shows the simulation results for an inlet pressure of p_0=289.9 Pa to match the calculation for 8mL of inlet media. The pressure head was applied directly to the center cross area z-coordinate of the channel on the XY-plane, where the channel connects to the inlet side of the middle well. A pressure of p=0 Pa, or atmospheric pressure, was applied to the top of the inlet and outlets to avoid flow resistance. A gravity constant was applied to the whole design. The side profile, displayed in **Figure 8(B) ,** shows that a combination of the aforementioned factors successfully simulated flow traveling down, through the channel, into the middle well containing the hydrogel, and out the connected outlet.

The side profiles shown in **Figures 8(C, D)** depict the gradient of velocity magnitudes for the same pressure impacted by the varying geometries of the outlets. The comparably high velocities on the channel directly over the inlet and outlet to the middle well were expected as there is a sharp decrease in volume in this part of the design; therefore, the pressure and flow velocity should increase. The gradients in the center of the gel initially appeared to have no flow going, but upon closer inspection, these were higher on the gradient scale than the outermost edges of the device, meaning that flow was simulated through the hydrogel phase of the device. The values on the gradient-scale legend match the point evaluation calculations done on the XY positions associated with the conditions in **table 3**. The point evaluations were done at the same z-position, where this coordinate was at the middle height of the channel cross-section. These values

appear small, being on the μm/s scale, but if this simulation turns out to be similar to actual flow in the device, the cells will still be experiencing a flow rate within the physiological range of interstitial fluid flow in humans (Munson & Shieh, 2014).

The point evaluation values in **table 3** were very close. It was expected that the difference in outlet geometry would cause a larger variation than simulated. The values show that the design changes did not impact flow physics. There may have been a slight difference, however, that depends on the x-position of the well and how pressure from the media is distributed from the inlet throughout the device. This variance will be kept in mind for future design expansion.

Table 3. Point evaluation for velocity magnitude at the center of gels for each condition and location.

Outlet Design and Position for Flow on Gel	Velocity Magnitude (m/s)	Velocity Magnitude (μm/s)
Reservoir 1	2.2045E-06	2.205
Reservoir 2	2.2067E-06	2.207
Well 1	2.2148E-06	2.215
Well 2	2.2020E-06	2.202

Viability of tumor cells on Formlabs Clear Resin Device

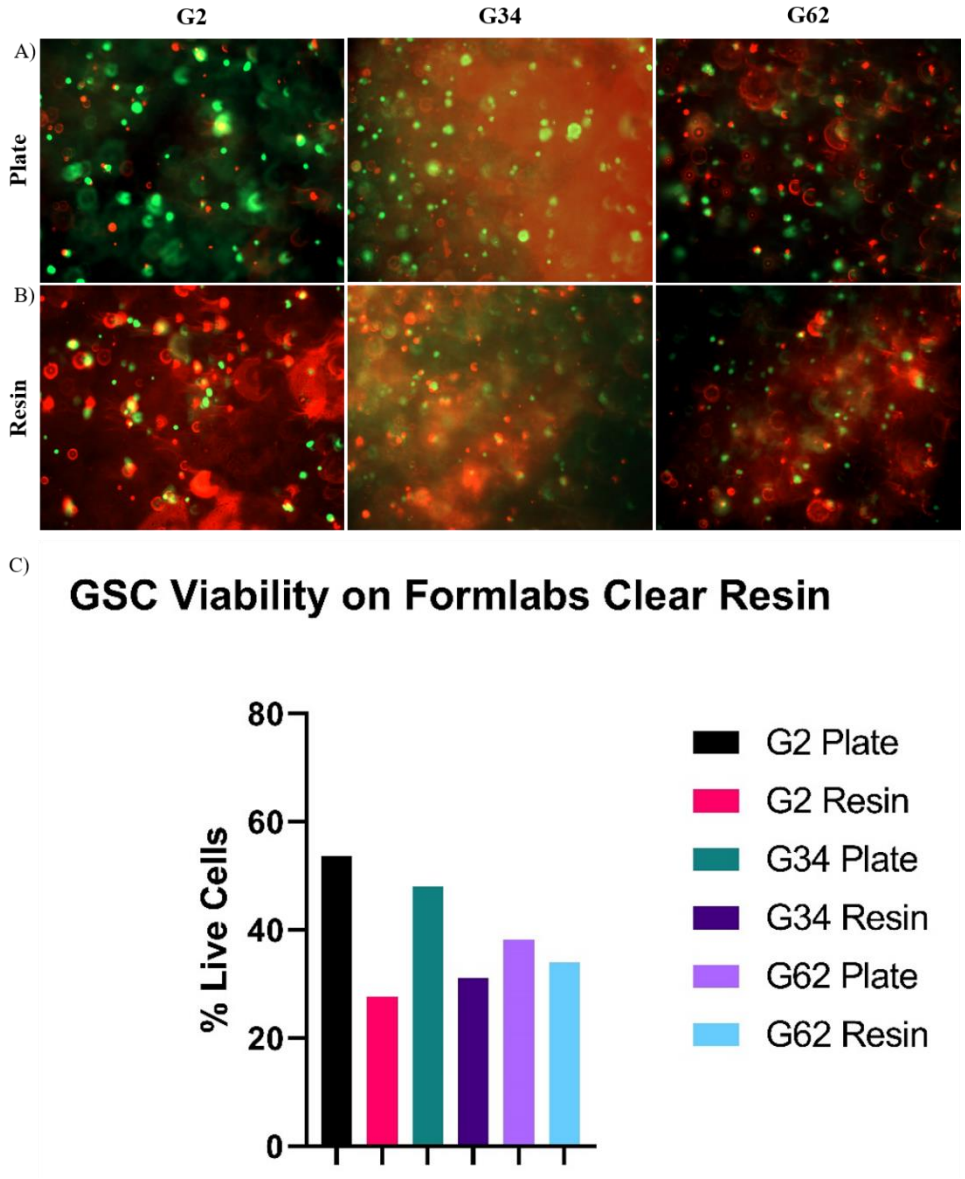

Figure 9. Viability of GSC lines. Cells were tested for viability in A) a low attachment well plate (Corning) and B) a Formlabs Clear resin for overnight (17 h) incubation. C) Live cell percentage averages (n=2) for cells encapsulated gels set in each material.

The average of two viability trials is shown in **Figure 9(C)**. A representative image at 100x total magnification is shown for live-dead labeling of cells in both conditions for three GSC lines, G2, G34, and G62, in **Figures 9(A, B)**. The images of cells were from the final trial, trial 3, where

gels were removed from both surfaces and placed between histology slides for imaging. Because the live and dead labels could not be distinguished in these images, the cells with a bright green center and no traces of red were counted as live cells. Cells that were entirely red or green with traces of red were counted as dead cells. Live and dead values were combined to get the total value of cells for calculating the live cell percentage. The total number of cells included cells fully in focus and those with a definable shape in the fluorescent channels.

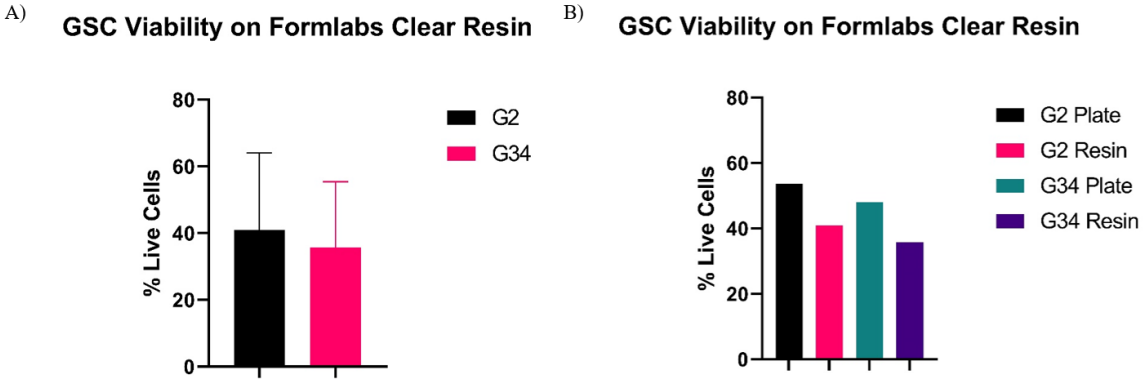

Figure 10. Viability of G2 and G34 cell lines. A) Shows the average of live cell percentage (n=3) for these cells just in the resin. B) Compares all of the results averages in (A) to the cell viability in the plate for each cell line shown in Figure 10(C).

Figure 10 shows the viability results using the G2 and G34 cell lines as a trial of just these two cell lines in resin was done before the trials depicted in **Figure 9**. No plate condition images were available for this trial as, at the time, the incorrect plate type had been used for incubating and attempting to image the cells. Nevertheless, this trial was included as another proof of concept that the cells can live in the resin, though at lower percentages than in a cell culture plate. These overall results could be accurate in the ideal scenario, and the post-print processing made the device bio-compatible while still being optimized. If this is not the case, then it is still expected

that a percentage of cells survive in the device overnight, though at a much lower rate than in the plate.

Cell motility tracking in standard conditions (gels in plate)

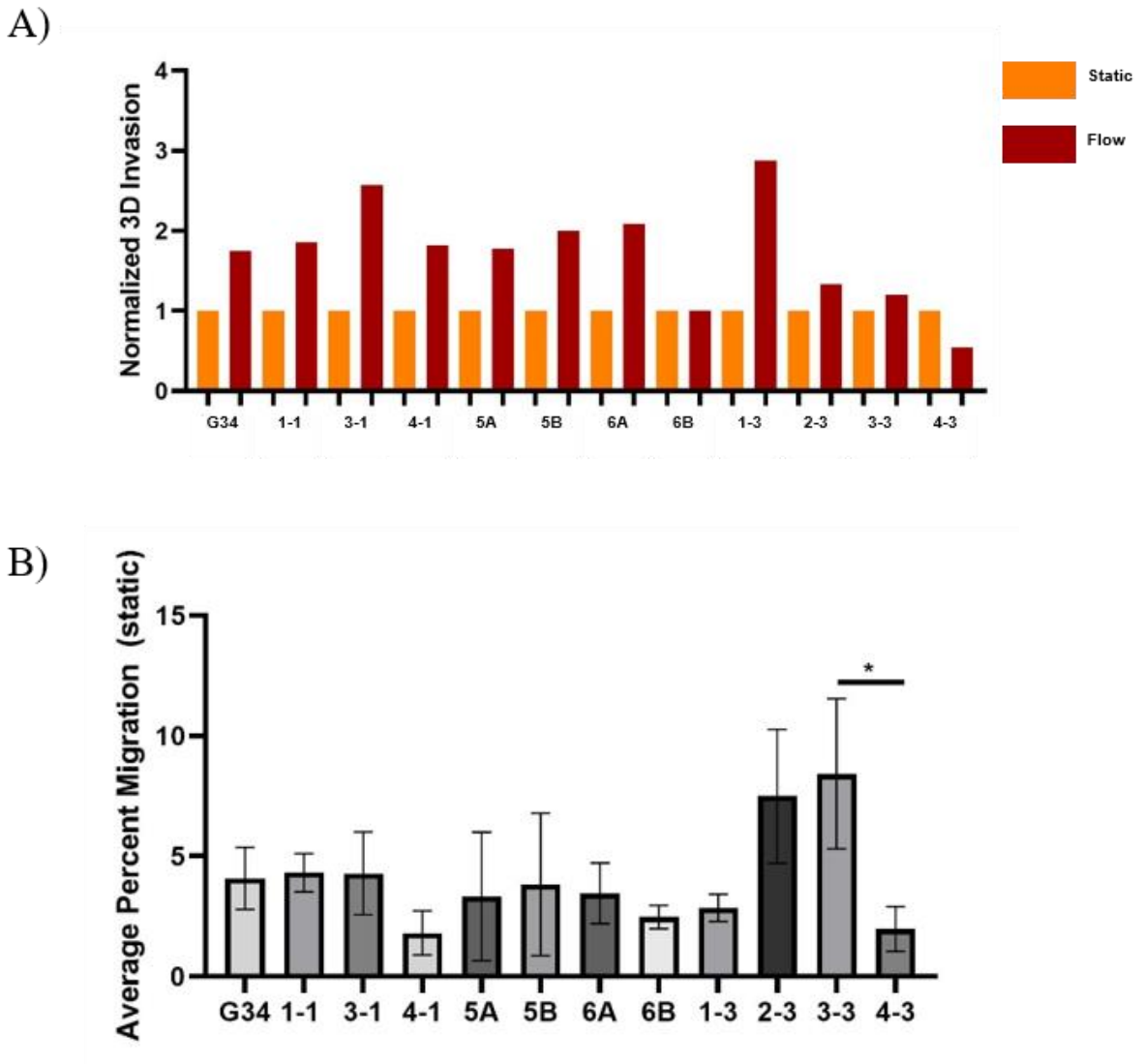

Figure 11. In vitro sub-clonal population static/flow & migratory characterization, courtesy of Monet Roberts, PhD. A) Normalized GSC sub-colony invasion percentages. These values were averages (n=7) of static flow invasion assays. Assays were set up in the same way as the 3D in vitro interstitial flow model (Kingsmore et al., 2016). B) Average percent migration (n=5) of sub-colony live imaging in a cell culture plate (Corning).

The results shown in **Figure 11** are part of the project the live-imaging device was initially intended for and were used to determine which cells to prioritize in the first successful iteration of the device. Many sub-colonies were previously isolated from the G34 patient-derived cell line. As previously mentioned, the G34 cell line was responsive to fluid flow, so sub-clones were expected to display similar behavior (Kingsmore et al., 2016). **Figure 11(A)** shows that most of these cells were more prone to invasion under flow than in static conditions. Two cells of interest were chosen based on the invasion results: the 1-3 G34 sub-colony for having the most invasive response and the 4-3 G34 sub-colony for having the least. The selected sub-colonies were also imaged on the IBIDI microfluidic as the resin device was optimized.

Live imaging was done on Vibrant Did labeled cells encapsulated in a hydrogel set in a cell culture plate. Cell imaging and static flow assays were done in parallel, but initial live imaging could only be done on cells under static conditions. The data from these overnight imaging sessions shown in **Figure 11(B)** provided more insight into sub-colony selection. In these results, the 3-3 line moved the most, and the 4-3 line was among those that moved the least. Surprisingly the 1-3 line did not migrate to the extent the 3-3 line did, but this did not entirely remove it as a candidate for imaging under flow conditions later. The 3-3 line was not identified in time to be included in the IBIDI microfluidic imaging in this paper, but it was included in the final resin device imaging.

Cell Motility under Static and Flow (IBIDI)

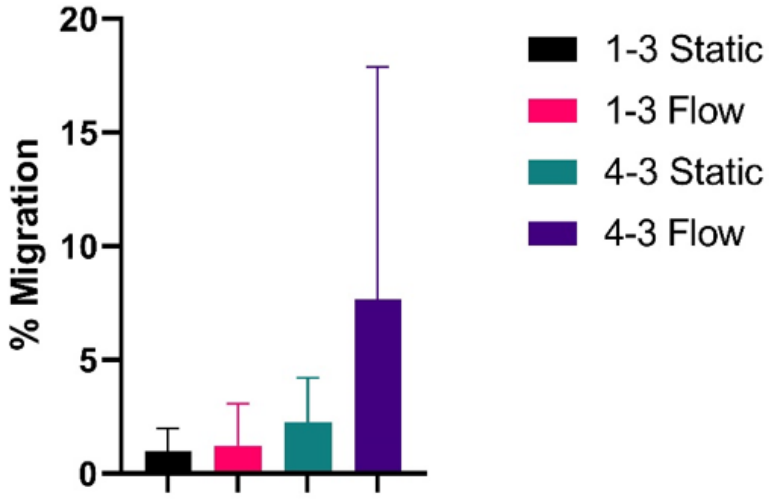

Figure 12. Average % Migration of GSC sub-colonies under static and flow conditions in IBIDI microfluidic. (n=3). Three ROIs at 200x magnification were analyzed per condition in each trial.

The IBIDI imaging results show a higher amount of cells moving under flow from the less flow-responsive cell line, which was much unexpected. Both cell lines did manage to have a higher percentage of moving cells under flow than in static conditions though this was expected to be a more drastic difference. A low amount of movement was detected in the 1-3 line.

Only the final three imaging lines were used for this analysis as previous runs had issues with tubing becoming detached, larger air bubbles appearing in the microfluidic overnight, the duration of imaging being impacted, or the cell density not being ideal for imaging. These final runs had the best distribution of cells, yet there were still regions in the OA that barely contained cells due to difficulty in controlling cell distribution in the OA. Drift that occurred while imaging and, potentially, the pressure from flow through the gel caused the gel to shake rapidly at times, impacting how individual cell movement was detected. The most accurate analysis was done by labeling cells at the beginning frame using the events tool under graphics in the Zen imaging

software (Zeiss) and determining which cells moved against the gel movement. It is difficult to determine if the results are reliable as, overall, more cell movement was detected in previous imaging runs while the setup was being optimized.

Cell Motility under Static and Flow (Resin Device Imaging)

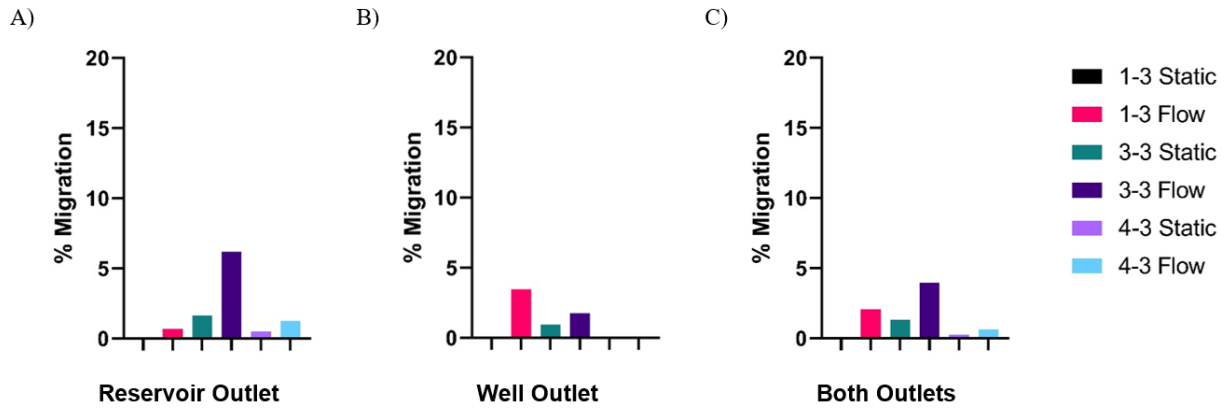

Figure 13. Average % Migration of GSC sub-colonies under static and flow conditions in resin live-imaging device (n=2). ROIs at 100x magnification were analyzed per condition in each trial. A) The average percent migration of each sub-colony of interest in the flow wells leading out to the reservoir outlet. B) The same data as (A) for the flow wells leading out to well outlets. C) The average percent migration under static and flow conditions for both designs.

The migration data obtained by imaging cells in the resin device was very similar to trends from cell imaging under standard conditions. Overall, more cell movement was seen for single cells under flow than in static conditions in every graph in **Figure 13**. The 4-3 line, or least flow-responsive, showed the least activity in both the static and flow conditions. The level of flow response switched in the 1-3 and 3-3 sub-colonies depending on the outlet design. The static response, as expected since these had the highest movement in previous static live-imaging, was the highest in the 3-3 line.

The graph with both designs averaged, **Figure 13(C)**, was created after the velocities through all these gels were calculated to be very similar on COMSOL. In this graph, it looks like the 3-3 line is more flow responsive than the 1-4 line, but given the results from the well outlet and previous invasion data, as well as the low n=2, this would require more trials to determine which is the ideal line to compare between cells lines of varying flow response. Nevertheless, the imaging results from this device offer a base for higher throughput live imaging because of the trends seen in static and flow migration percentages. No imaging was done in the device with the parental G34 cell line, but this is planned as a future step, and it is expected to have migration values within the range of these sub-colonies. Further cell-tracking analysis and flow tests are ongoing to better determine if the exposure to flow in this device is the cause of these differences between conditions.

Discussion

Summary of Results

A printable and easy-to-modify device was developed that successfully generated flow through a hydrogel without using pumps. The device was biocompatible as a percentage of cells were labeled by a live stain after incubating in the device overnight, and cells were motile in the device while imaging. Sub-colonies of interest from a flow-responsive GSC were imaged on this device, and results showed promise in developing a higher throughput method for studying them comparable to current imaging standards.

Analysis of results

Final design of chamber

While using this version of the device, there were still issues of leaking to address. At the end of some of the overnight imaging, there was media leaked and dried around the base of the device. The bottom seal of the device was tested before the final sterile PBS bath, but there is concern that it is either not remaining intact through the bath or the imaging. For the first potential cause, the PBS and heat could be undoing the seal, but the silicone is supposed to be waterproof, so the main issue could be how long the silicone is allowed to cure before placing it in the bath. This scenario might be the least probable cause because the media should immediately leak from the device when applied for flow. The other scenario that could be causing this is the stage-top of the device moving too much while imaging occurs overnight. There were no problems for the first few hours of imaging, but at some point, well into the experiment, the image quality changed and part of this could be a leak occurring. The stage top moving to different positions could eventually

lead to the microscope hitting the bottom of the device and insufficient space on top of the device for it to move upward. The movement while imaging could also lead to media making contact with the parafilm covering the device and rolling down the side of the device by adhesion because often the parafilm is stained with dry media or still wet with media at the end of experiments.

Despite these seal issues, an increase in media was observed in the outlets at the end of the experiments. Therefore, exact flow measurements will need to be performed to determine the flow velocity at the beginning of the media application and throughout the duration of a live-imaging experiment. Attempts at this had been made by trying to perform a fluorescence recovery after photo-bleaching (FRAP) assay using dextran and a spinning disk confocal. However, the application of dextran was difficult with the slow flow rate. Dextran was diluted too much to see any of this travel through the gel when applied to the inlet, and when applied on top of the gel, it was too bright to get any recovery images. The timing of dextran application on top of the gel must be determined for the ideal amount of this to be in the gel such that a photo-bleached region can be created and flow can be measured. Fluorescent microbeads were also tried at the beginning of flow tests on the device, and it was determined that these would not travel past the channel opening into the gel. A positive interpretation of this was that the resin surface and gel formed a good seal for flow to only occur through the gel. At the time the microbeads were initially used, there was no flow going through a hydrogel in the device, so now that a successful flow device design has been established, this method could be attempted again with microbeads of varying sizes.

COMSOL modeling of flow through the chamber

The values calculated in the simulation and point evaluations were only for the start of flow when media is first applied to the inlet. These exact calculations would be expected to decrease as media volume decreases on the inlet over time. However, with the calculated velocity, this is not expected to decrease to a velocity that reaches 0 μm/s over the duration of live imaging. This concern will be applied to future simulations along with measurements of flow taken in real-time of media in the device to compare.

Viability of tumor cells in the chamber

In the initial trials imaged for cell viability, gels remained in the plate and resin device while imaging and this caused issues with image clarity, especially in the resin device. The images taken in the plate for the first trial were clear in the fluorescent channels but not so clear in brightfield. The images taken in the resin device were very clear in brightfield, cells were somewhat distinguishable in the EGFP green channel, and cells were barely or not visible in the EtHD1 red channel like they were in the final trial. Background subtraction was applied as a post-processing step in the trials imaged directly in the resin device; this marginally improved the cell visibility in the green channel. Issues in the green channel were explained by fluorescent intensity tests done on this resin, revealing that the resin moderately auto-fluoresced in this channel (Musgrove et al., 2022). Data was unavailable for a channel like the red channel used for the dead stain, and images were less clear in this channel than in the green one. Potential reasons could be that the resin auto-fluoresced more in this channel, there was an issue with light scattering in the resin, or the dead stain leached into the resin. The way the device was oriented on the microscope

and the z-position selected for focus were not probably reasons for the unclear images because the brightfield acquisition showed cells were in focus. However, due to the aforementioned variability in clarity for each channel, the resulting images were all analyzed in different ways that depended on their visibility. This analysis could have skewed the final results for comparison but imaging tests performed after this determined that cells were moving, so some were alive for analysis. Unfortunately, contamination occurred in one of the cell lines at the time, preventing another trial from being performed before cells were live-imaged moving in the device. More viability tests might be needed as these trials were done while post-print processing was still being optimized, and cell visibility issues were finally addressed with the final viability trial.

Cell motility in each imaging set-up

The variety of behaviors seen in the sub-colonies from the experiments done on standard conditions is still being interpreted in comparison to the parental colony. More imaging trials need to occur for the device to reach similar use, especially with the inclusion of the parental colony.

The need for a pumpless imaging setup was further established upon practice using the microfluidic pump setup for imaging comparisons. There was a limit to one chip being imaged at a time due to the space allowed for tubing to run through the stage-top incubator. The issue of a secure seal was also evident, as this part took the longest when optimizing the IBIDI chip. It was expected for this to take less time, and similar problems have occurred with other PDMS microfluidics. The chip's geometry also leads to experimental use issues due to the relatively small OA for imaging. Applying the gel on its own was variable because sometimes there was an excellent distribution of cells in the OA and sometimes most of the cells collected at both ports

where they could not be imaged for flow. This channel's vertical size was also much smaller than the media reservoirs on the sizes. This feature was ideal for the intended use of the device. For flow, however, this feature would lead to the pressure from applying the tubing sometimes being too high in this region, and the gel would rip. This kept occurring when FRAP trials were attempted leading to the likelihood that the same was occurring during live imaging runs despite little to no tears being visible in the OA for the analyzed trials. The gel being un-adhered or torn might have been why the results were not similar to cell behaviors seen in standard conditions.

The resin device took a while to process for biocompatibility after being printed, and because of this, it did not offer the same initial convenience as the pre-made biocompatible IBIDI microfluidic. Despite this, the setup without pumps proved the resin device a more time-efficient setup on experiment days. Once more trials are done with this, and the cause of leaks in the device is addressed, it would be nice to see if the results remain similar to what was seen in standard invasion assays.

Future Directions

The current microfluidic has two outlet designs; once FRAP can be done on this to see if the flow through gels in both designs is similar, one of them will be chosen as the main design. It is desired to expand this design so that more wells experience flow. With an expansion would come finding a more efficient way to attach the device to an imaging surface and obtaining imaging surfaces compatible in size with the larger device and the stage-top incubator. Impacts to flow with expansion modifications on the inlet should also be monitored depending on how these are done. If the COMSOL simulation is close to what is physically occurring in the device, an osmotic agent

could be added to the setup to create higher fluid flow velocities while keeping the compact design that fits in the stage-top incubator.

Though a plug cover was used during these first attempts, a removable cover with a good seal is one of the next design features that would be ideal if the parafilm is causing media to come out while imaging. Additionally, it would be ideal to have a mechanism to keep cells sterile while imaging while also being able to access these in the future with microdissection techniques.

Only a few sub-colonies for one GSC were studied with the device. Hopefully, the future design expansion will allow for more sub-colonies of the same parental line to be imaged simultaneously under similar flow conditions. Finally, it would be ideal to ultimately run this device's imaging in parallel to a standard static flow invasion assay and determine if motile behaviors correlate this way.

Other Potential Applications

The potential of pumpless flow in a hydrogel could be used to study multiple functions in the body. Use to image cells from other types of cancer and the impacts of treatment application could be future implementations. Cell motility is essential in other functions of the body, such as wound healing and the immune system, so the removal and addition of flow with varying conditions would also be interesting to try. Current work in the lab concerning the glymphatic clearance system, Alzheimer's, Car-T cell therapy, the tumor microenvironment, or the lymphatic system might also be studied with alterations to the resin live-imaging device. It would be ideal to optimize the imaging setup with this device and go back to do imaging of other GSCs before expanding to other applications. If microdissection is compatible with the device, it could also be

used in the reverse application of sub-colony imaging and instead used to image parental lines from which sub-colonies are obtained for expansion.

References

About Glioblastoma. (n.d.). Retrieved November 16, 2022, from https://braintumor.org/events/glioblastoma-awareness-day/about-glioblastoma/

Aghamiri, S., Rabiee, N., Ahmadi, S., Rabiee, M., Bagherzadeh, M., & Karimi, M. (2021). Microfluidic devices: Synthetic approaches. In *Biomedical Applications of Microfluidic Devices* (pp. 23–36). Elsevier. https://doi.org/10.1016/B978-0-12-818791-3.00003-6

Bhattacharjee, N., Urrios, A., Kang, S., & Folch, A. (2016). The upcoming 3D-printing revolution in microfluidics. *Lab on a Chip*, *16*(10), 1720–1742. https://doi.org/10.1039/C6LC00163G

Bonnet, D., & Dick, J. E. (1997). Human acute myeloid leukemia is organized as a hierarchy that originates from a primitive hematopoietic cell. *Nature Medicine*, *3*(7), 730–737. https://doi.org/10.1038/NM0797-730

Cell Culture Media Supplements | Thermo Fisher Scientific - US. (n.d.). Retrieved November 21, 2022, from https://www.thermofisher.com/us/en/home/life-science/cell-culture/mammalian-cell-culture/media-supplements.html

Cornelison, R. C., Yuan, J. X., Tate, K. M., Petrosky, A., Beeghly, G. F., Bloomfield, M., Schwager, S. C., Berr, A. L., Stine, C. A., Cimini, D., Bafakih, F. F., Mandell, J. W., Purow, B. W., Horton, B. J., & Munson, J. M. (2022). A patient-designed tissue-engineered model of the infiltrative glioblastoma microenvironment. *Npj Precision Oncology*, *6*(1), 54. https://doi.org/10.1038/s41698-022-00290-8

Corning® 3374 HTS Transwell® 96 Permeable Support Culture Plate System with. (n.d.). Retrieved October 28, 2022, from https://www.capitolscientific.com/Corning-3374-HTS-Transwell-96-Permeable-Support-Culture-Plate-System-with-96-Well-Insert-Unit-R

Corning | Materials Science Technology and Innovation. (n.d.). Retrieved November 16, 2022, from https://www.corning.com/worldwide/en.html

Cupping blowout. (n.d.). Retrieved October 29, 2022, from https://support.formlabs.com/s/article/Cupping-Blowout?language=en_US

de Almeida Monteiro Melo Ferraz, M., Nagashima, J. B., Venzac, B., le Gac, S., & Songsasen, N. (2020). 3D printed mold leachates in PDMS microfluidic devices. *Scientific Reports*, *10*(1), 994. https://doi.org/10.1038/s41598-020-57816-y

Delpech, B., Maingonnat, C., Girard, N., Chauzy, C., Olivier, A., Maunoury, R., Tayot, J., & Creissard, P. (1993). Hyaluronan and hyaluronectin in the extracellular matrix of human brain tumour stroma. *European Journal of Cancer (Oxford, England : 1990)*, *29A*(7), 1012–1017. https://doi.org/10.1016/S0959-8049(05)80214-X

Duffau, H. (2017). Les glioblastomes en 2017. *La Revue de l'Infirmière*, *66*(228), 16–18. https://doi.org/10.1016/j.revinf.2016.12.002

Femmer, T., Jans, A., Eswein, R., Anwar, N., Moeller, M., Wessling, M., & Kuehne, A. J. C. (2015). High-Throughput Generation of Emulsions and Microgels in Parallelized Microfluidic Drop-Makers Prepared by Rapid Prototyping. *ACS Applied Materials & Interfaces*, *7*(23), 12635–12638. https://doi.org/10.1021/acsami.5b03969

Fleck, E., Sunshine, A., Denatale, E., Keck, C., McCann, A., & Potkay, J. (2021). Advancing 3d-printed microfluidics: Characterization of a gas-permeable, high-resolution pdms resin for stereolithography. *Micromachines*, *12*(10). https://doi.org/10.3390/mi12101266

Furth, J., & Kahn, M. C. (1937). The Transmission of Leukemia of Mice with a Single Cell. *The American Journal of Cancer*, *31*(2), 276–282. https://doi.org/10.1158/AJC.1937.276

Galarza, S., Kim, H., Atay, N., Peyton, S. R., & Munson, J. M. (2020). 2D or 3D? How cell motility measurements are conserved across dimensions in vitro and translate in vivo. *Bioengineering and Translational Medicine*, *5*(1). https://doi.org/10.1002/btm2.10148

Gimple, R. C., Bhargava, S., Dixit, D., & Rich, J. N. (2019). Glioblastoma stem cells: lessons from the tumor hierarchy in a lethal cancer. *Genes & Development*, *33*(11–12), 591–609. https://doi.org/10.1101/gad.324301.119

Gliomas | Johns Hopkins Medicine. (n.d.). Retrieved November 16, 2022, from https://www.hopkinsmedicine.org/health/conditions-and-diseases/gliomas

Gong, H., Bickham, B. P., Woolley, A. T., & Nordin, G. P. (2017). Custom 3D printer and resin for 18 µm × 20 µm microfluidic flow channels. *Lab on a Chip*, *17*(17), 2899–2909. https://doi.org/10.1039/C7LC00644F

Halldorsson, S., Lucumi, E., Gómez-Sjöberg, R., & Fleming, R. M. T. (2015). Advantages and challenges of microfluidic cell culture in polydimethylsiloxane devices. *Biosensors and Bioelectronics*, *63*, 218–231. https://doi.org/10.1016/j.bios.2014.07.029

Hanahan, D., & Weinberg, R. A. (2000). The hallmarks of cancer. *Cell*, *100*(1), 57–70. https://doi.org/10.1016/S0092-8674(00)81683-9

Hanahan, D., & Weinberg, R. A. (2011). Hallmarks of Cancer: The Next Generation. *Cell*, *144*(5), 646–674. https://doi.org/10.1016/J.CELL.2011.02.013

Hemmati, H. D., Nakano, I., Lazareff, J. A., Masterman-Smith, M., Geschwind, D. H., Bronner-Fraser, M., & Kornblum, H. I. (2003). Cancerous stem cells can arise from pediatric brain tumors. *Proceedings of the National Academy of Sciences of the United States of America*, *100*(25), 15178. https://doi.org/10.1073/PNAS.2036535100

Hill, R. G. (2005). Polymers. *Biomaterials, Artificial Organs and Tissue Engineering*, 37–47. https://doi.org/10.1533/9781845690861.1.37

Hwang, H. H., Zhu, W., Victorine, G., Lawrence, N., & Chen, S. (2018). 3D-Printing of Functional Biomedical Microdevices via Light- and Extrusion-Based Approaches. *Small Methods*, *2*(2), 1700277. https://doi.org/10.1002/smtd.201700277

Jackson, C. M., Choi, J., & Lim, M. (2019). Mechanisms of immunotherapy resistance: lessons from glioblastoma. *Nature Immunology*, *20*(9), 1100–1109. https://doi.org/10.1038/s41590-019-0433-y

Jans, A., Lölsberg, J., Omidinia-Anarkoli, A., Viermann, R., Möller, M., de Laporte, L., Wessling, M., & Kuehne, A. J. C. (2019). High-Throughput Production of Micrometer Sized Double Emulsions and Microgel Capsules in Parallelized 3D Printed Microfluidic Devices. *Polymers*, *11*(11), 1887. https://doi.org/10.3390/polym11111887

Kim, J., Lee, I.-H., Cho, H. J., Park, C.-K., Jung, Y.-S., Kim, Y., Nam, S. H., Kim, B. S., Johnson, M. D., Kong, D.-S., Seol, H. J., Lee, J.-I., Joo, K. M., Yoon, Y., Park, W.-Y., Lee, J., Park, P. J., & Nam, D.-H. (2015). Spatiotemporal Evolution of the Primary Glioblastoma Genome. *Cancer Cell*, *28*(3), 318–328. https://doi.org/10.1016/j.ccell.2015.07.013

Kingsmore, K. M., Logsdon, D. K., Floyd, D. H., Peirce, S. M., Purow, B. W., & Munson, J. M. (2016). Interstitial flow differentially increases patient-derived glioblastoma stem cell invasion via CXCR4, CXCL12, and CD44-mediated mechanisms. *Integrative Biology*, *8*(12), 1246–1260. https://doi.org/10.1039/C6IB00167J

Kingsmore, K. M., Vaccari, A., Abler, D., Cui, S. X., Epstein, F. H., Rockne, R. C., Acton, S. T., & Munson, J. M. (2018). MRI analysis to map interstitial flow in the brain tumor microenvironment. *APL Bioengineering*, *2*(3). https://doi.org/10.1063/1.5023503

Lake, J. R., Heyde, K. C., & Ruder, W. C. (2017). Low-cost feedback-controlled syringe pressure pumps for microfluidics applications. *PloS One*, *12*(4), e0175089. https://doi.org/10.1371/journal.pone.0175089

Lapidot, T., Sirard, C., Vormoor, J., Murdoch, B., Hoang, T., Caceres-Cortes, J., Minden, M., Paterson, B., Caligiuri, M. A., & Dick, J. E. (1994). A cell initiating human acute myeloid leukaemia after transplantation into SCID mice. *Nature*, *367*(6464), 645–648. https://doi.org/10.1038/367645A0

Lee, J., Kotliarova, S., Kotliarov, Y., Li, A., Su, Q., Donin, N. M., Pastorino, S., Purow, B. W., Christopher, N., Zhang, W., Park, J. K., & Fine, H. A. (2006). Tumor stem cells derived from glioblastomas cultured in bFGF and EGF more closely mirror the phenotype and genotype of primary tumors than do serum-cultured cell lines. *Cancer Cell*, *9*(5), 391–403. https://doi.org/10.1016/j.ccr.2006.03.030

Linninger, A. A., Tsakiris, C., Zhu, D. C., Xenos, M., Roycewicz, P., Danziger, Z., & Penn, R. (2005). Pulsatile Cerebrospinal Fluid Dynamics in the Human Brain. *IEEE Transactions on Biomedical Engineering*, *52*(4), 557–565. https://doi.org/10.1109/TBME.2005.844021

Männel, M. J., Fischer, C., & Thiele, J. (2020). A Non-Cytotoxic Resin for Micro-Stereolithography for Cell Cultures of HUVECs. *Micromachines 2020, Vol. 11, Page 246*, *11*(3), 246. https://doi.org/10.3390/MI11030246

McAvoy, K., Jones, D., & Thakur, R. R. S. (2018). Synthesis and Characterisation of Photocrosslinked poly(ethylene glycol) diacrylate Implants for Sustained Ocular Drug Delivery. *Pharmaceutical Research*, *35*(2). https://doi.org/10.1007/S11095-017-2298-9

McDonald, J. C., & Whitesides, G. M. (2002). Poly(dimethylsiloxane) as a Material for Fabricating Microfluidic Devices. *Accounts of Chemical Research*, *35*(7), 491–499. https://doi.org/10.1021/ar010110q

Munson, J. M., Bellamkonda, R. v., & Swartz, M. A. (2013). Interstitial flow in a 3d microenvironment increases glioma invasion by a cxcr4-dependent mechanism. *Cancer Research*, *73*(5), 1536–1546. https://doi.org/10.1158/0008-5472.CAN-12-2838/650595/AM/INTERSTITIAL-FLOW-IN-A-3D-MICROENVIRONMENT

Munson, J. M., & Shieh, A. C. (2014). Interstitial fluid flow in cancer: implications for disease progression and treatment. *Cancer Management and Research*, *6*(1), 317–328. https://doi.org/10.2147/CMAR.S65444

Munthe, S., Petterson, S. A., Dahlrot, R. H., Poulsen, F. R., Hansen, S., & Kristensen, B. W. (2016). Glioma Cells in the Tumor Periphery Have a Stem Cell Phenotype. *PLoS ONE*, *11*(5), e0155106. https://doi.org/10.1371/JOURNAL.PONE.0155106

Musgrove, H. B., Catterton, M. A., & Pompano, R. R. (2022). Applied tutorial for the design and fabrication of biomicrofluidic devices by resin 3D printing. *Analytica Chimica Acta*, *1209*, 339842. https://doi.org/10.1016/J.ACA.2022.339842

Narayanamurthy, V., Jeroish, Z. E., Bhuvaneshwari, K. S., Bayat, P., Premkumar, R., Samsuri, F., & Yusoff, M. M. (2020). Advances in passively driven microfluidics and lab-on-chip devices: a comprehensive literature review and patent analysis. *RSC Advances*, *10*(20), 11652–11680. https://doi.org/10.1039/D0RA00263A

Poly Vinyl Alcohol - an overview | ScienceDirect Topics. (n.d.). Retrieved October 29, 2022, from https://www.sciencedirect.com/topics/materials-science/poly-vinyl-alcohol

Polydimethylsiloxane - an overview | ScienceDirect Topics. (n.d.). Retrieved October 28, 2022, from https://www.sciencedirect.com/topics/chemical-engineering/polydimethylsiloxane

Preventing suction cups in PreForm. (n.d.). Retrieved October 29, 2022, from https://support.formlabs.com/s/article/Preventing-suction-cups-in-PreForm?language=en_US

Singh, S. K., Clarke, I. D., Terasaki, M., Bonn, V. E., Hawkins, C., Squire, J., & Dirks, P. B. (2003). Identification of a cancer stem cell in human brain tumors. *Cancer Research*, *63*(18), 5821–5828.

Singh, S. K., Hawkins, C., Clarke, I. D., Squire, J. A., Bayani, J., Hide, T., Henkelman, R. M., Cusimano, M. D., & Dirks, P. B. (2004). Identification of human brain tumour initiating cells. *Nature*, *432*(7015), 396–401. https://doi.org/10.1038/NATURE03128

Stone, H. A., & Kim, S. (2001). Microfluidics: Basic issues, applications, and challenges. In *AIChE Journal* (Vol. 47, Issue 6). https://doi.org/10.1002/aic.690470602

Swartz, M. A., & Lund, A. W. (2012). Lymphatic and interstitial flow in the tumour microenvironment: linking mechanobiology with immunity. *Nature Reviews Cancer 2012 12:3*, *12*(3), 210–219. https://doi.org/10.1038/nrc3186

Tan, A. C., Ashley, D. M., López, G. Y., Malinzak, M., Friedman, H. S., & Khasraw, M. (2020). Management of glioblastoma: State of the art and future directions. *CA: A Cancer Journal for Clinicians*, *70*(4), 299–312. https://doi.org/10.3322/caac.21613

Tykocki, T., & Eltayeb, M. (2018). Ten-year survival in glioblastoma. A systematic review. *Journal of Clinical Neuroscience*, *54*, 7–13. https://doi.org/10.1016/j.jocn.2018.05.002

Utada, A. S., Lorenceau, E., Link, D. R., Kaplan, P. D., Stone, H. A., & Weitz, D. A. (2005). Monodisperse double emulsions generated from a microcapillary device. *Science*, *308*(5721), 537–541. https://doi.org/10.1126/SCIENCE.1109164/SUPPL_FILE/UTADA.SOM.PDF

Wagner, M., & Wiig, H. (2015). Tumor interstitial fluid formation, characterization, and clinical implications. *Frontiers in Oncology*, *5*(MAY), 115. https://doi.org/10.3389/FONC.2015.00115/BIBTEX

Weller, M., & le Rhun, E. (2020). How did lomustine become standard of care in recurrent glioblastoma? *Cancer Treatment Reviews*, *87*, 102029. https://doi.org/10.1016/j.ctrv.2020.102029

Wells, A., Grahovac, J., Wheeler, S., Ma, B., & Lauffenburger, D. (2013). Targeting tumor cell motility as a strategy against invasion and metastasis. *Trends in Pharmacological Sciences*, *34*(5), 283. https://doi.org/10.1016/J.TIPS.2013.03.001

Wirsching, H.-G., Galanis, E., & Weller, M. (2016). *Glioblastoma* (pp. 381–397). https://doi.org/10.1016/B978-0-12-802997-8.00023-2

Xiong, L., Chen, P., & Zhou, Q. (2014). Adhesion promotion between PDMS and glass by oxygen plasma pre-treatment. *Journal of Adhesion Science and Technology*, *28*(11). https://doi.org/10.1080/01694243.2014.883774